



CHEMISTRY

A European Journal

A Journal of



Accepted Article

Title: Advances in Porous Organic Polymers for Efficient Water Capture

Authors: Yearin Byun, Sang Hyun Je, Siddulu Naidu Talapaneni, and Ali Coskun

This manuscript has been accepted after peer review and appears as an Accepted Article online prior to editing, proofing, and formal publication of the final Version of Record (VoR). This work is currently citable by using the Digital Object Identifier (DOI) given below. The VoR will be published online in Early View as soon as possible and may be different to this Accepted Article as a result of editing. Readers should obtain the VoR from the journal website shown below when it is published to ensure accuracy of information. The authors are responsible for the content of this Accepted Article.

To be cited as: *Chem. Eur. J.* 10.1002/chem.201900940

Link to VoR: <http://dx.doi.org/10.1002/chem.201900940>

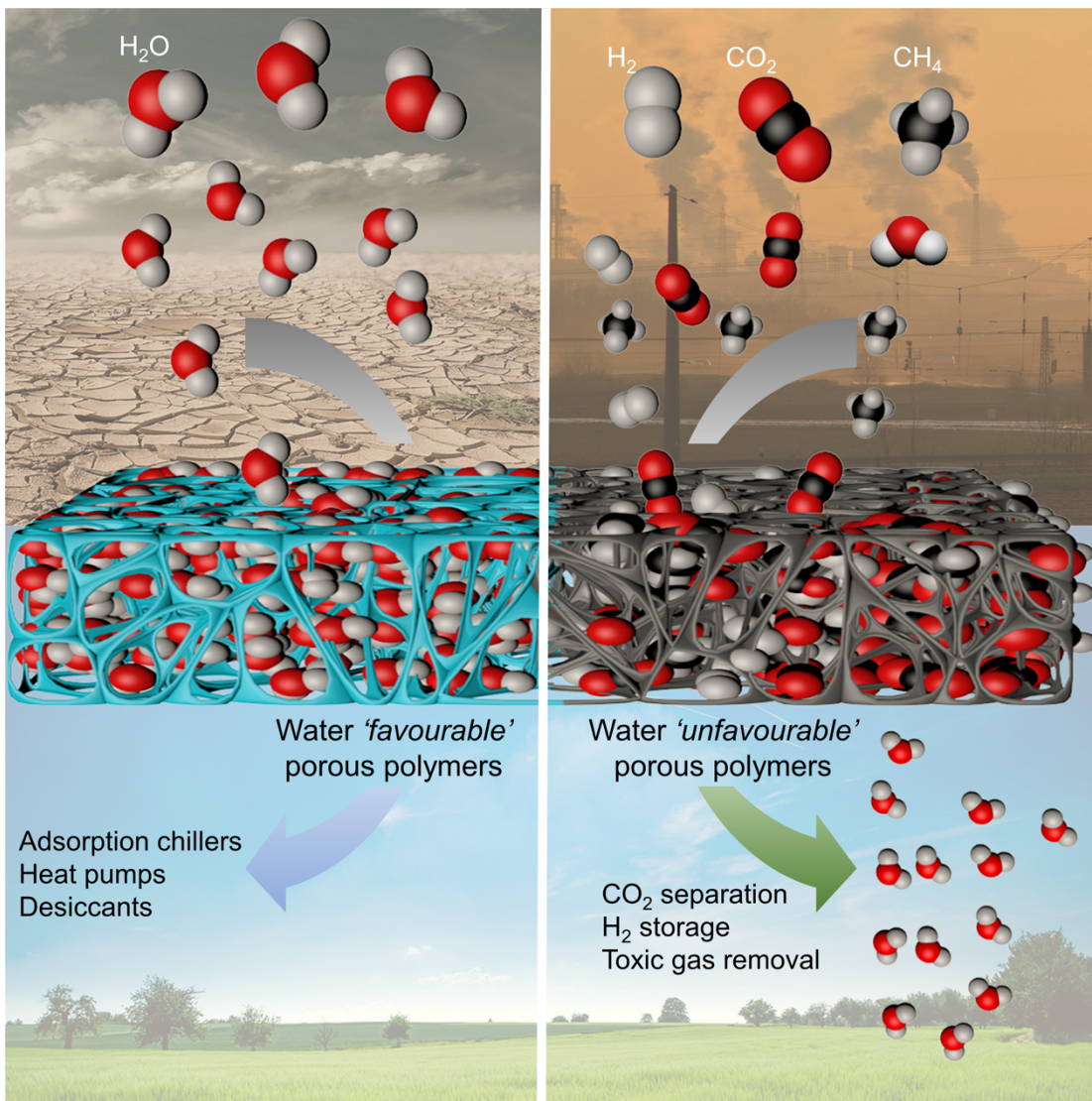
Supported by
ACES

WILEY-VCH

REVIEW

Advances in Porous Organic Polymers for Efficient Water Capture

Yearin Byun^{+[a]}, Sang Hyun Je^{+[a]}, Siddulu Naidu Talapaneni^{+[a]} and Ali Coskun*^[a,b]



REVIEW

Abstract: Desiccant driven dehumidification for maintaining the proper humidity levels and atmospheric water capture with minimum energy penalty are important aspects in heat pumps, refrigeration, gas and liquid purifications, gas sensing, and clean water production for improved human health and comfort. Water adsorption using nanoporous materials has emerged as a viable alternative to energy intensive industrial processes, thus understanding the significance of their porosity, high surface areas, vast pore volumes, chemical and structural features relative to the water adsorption is quite important. In this review article, we present important features of nanoporous materials including zeolites, porous carbons as well as crystalline and amorphous porous organic polymers (POPs) to define the interactions between the water molecules and the polar/non-polar functional groups on the surface of these nanoporous materials. In particular, we focused on the recent developments in POPs in the context of water capture due to their remarkable stability towards water and wide range of available synthetic routes and building blocks for their synthesis. We also highlighted recent approaches to increase the water sorption capacity of POPs by modifying their structure, morphology, porosity and chemical functionality while emphasizing their promising future in this emerging area.

1. Introduction

Efficient storage of substances can be regarded as the most essential technology that has been developed by humans. Unlike in the past, when the materials were stored using 'large vessels', it became very important in modern science with the advances in nanotechnology to develop ways to store small and light substances in large quantities. Accordingly, porous materials with tunable pore sizes and functionality have received a great deal of attention. In particular, porous materials such as activated carbon,^[1] zeolite,^[2] metal-organic frameworks (MOFs),^[3] covalent organic frameworks (COFs),^[4] porous organic polymers (POPs),^[5] present extremely high specific surface areas and also the advantage of capturing and storing various types of materials ranging from solid and liquid substances (i.e. nanoparticle,^[6] biosynthetic enzymes,^[7] oil spills^[8]) to gaseous substances. Gas capture and storage is among the most representative research areas where porous materials have been applied for several years. POPs both in crystalline and amorphous forms offer unique advantages due to their light-weight, low-cost, high stability and tunability. The gas capture and separation performance of POPs can be easily altered by varying organic building blocks or their functional groups. In addition, favourable textural properties of

these polymers such as high microporosity (pore size < 2 nm)^[9] significantly improve the binding affinity towards the guest molecules due to the fact that multiple binding sites can simultaneously interact with the guests through various noncovalent interactions. Accordingly, POPs have been widely investigated as adsorbents for the storage of small, environmentally-significant, gas molecules such as carbon dioxide, methane, hydrogen and toxic gases. More recently, it has also been shown that POPs can act as efficient desiccants to capture moisture from ambient air or under humid conditions. This particular research area is quite important considering the uneven distribution of clean water sources in the world. In principle, POPs can be utilized to capture atmospheric water and its subsequent regeneration using solar heat can eliminate the geographic limitations for access to clean water. In addition, humidity control is essential for our everyday life. For example, in the hospitals, the risk of infection is directly associated with the humidity levels, that is low or high humidity can increase infection risks through bacteria or virus. In industrial applications, water capture is critical in the manufacturing of moisture sensitive products such as semiconductors, pharmaceuticals and electric/electronic products. Furthermore, in energy production, a small amount of water could also play a negative role in energy efficiency, particularly in the processes such as (1) natural gas purification,^[10] (2) flue gas separation, (3) air separation,^[11] and (4) biofuel or diesel production.^[12] These processes generally contain moisture from ppm levels up to 40 wt%, which should be eliminated for proper operation. Therefore, it is highly important to develop an efficient 'humidity controlling agent' that can selectively adsorb moisture under various conditions.

There is a tremendous interest in maintaining proper humidity levels in air for the protection of entire eco system.^[13] The development of environmentally friendly advanced technologies for the adsorption of water vapor under different conditions coupled with the preparation of novel materials with improved uptake properties, recycling possibilities and long-term use are enduring tasks.^[14] To date, many inorganic adsorbents, namely, metal salts, zeolites, activated alumina and MOFs have been widely used as moisture adsorbents. The most well-known and easy-to-use drying agents are metal salts such as LiBr, LiCl, KBr, CaCl₂, and MgCl₂, however, their irreversible water sorption, high solubility in water and tendency to crystallize at high humidity levels make it difficult to use them as reversible moisture adsorbents. Although there have been several attempts to use metal hydroxides such as NaOH, KOH, CsOH instead of metal salts, their implementation in actual processes is still difficult since they melt at high humidity levels and lose their adsorption properties. Zeolites and activated alumina are the most widely used materials for dehumidification, however, their thermal regeneration step requires a very high energy input, with temperatures as high as 250–350 °C.^[15] Recently, MOFs have been utilized in water sorption applications.^[16] However, the limited availability of water-stable MOFs and their relatively high cost are still important factors to be considered for large-scale applications. In this regard, POPs are promising alternatives for humidity control, owing to their low-cost, good physicochemical stability and relatively lower regeneration temperatures. In this mini-review, we will first introduce critical factors for water vapor adsorption and then critically evaluate conventional water adsorbents such as zeolites and activated carbon, and finally

[a] Dr. Y. Byun, Dr. S. H. Je, Dr. S. N. Talapaneni and Prof. A. Coskun
Graduate School of EEWS, Korea Advanced Institute of Science
and Technology (KAIST), Daejeon 34141, Republic of Korea

[b] Prof. A. Coskun
Department of Chemistry, University of Fribourg, Chemin de Musee
9, Fribourg 1700, Switzerland.
E-mail: ali.coskun@unifr.ch

[*] These authors contributed equally to this work.

REVIEW

Yearin Byun obtained her BSc degree in chemistry from University of Maryland-College Park in 2013, and received her PhD in 2017 from Department of Energy Environment Water Sustainability (EEWS) at Korea Advanced Institute of Science and Technology (KAIST), South Korea, under the supervision of Prof. Ali Coskun. She is currently working as a post-doctoral researcher with Prof. Sang Ouk Kim in KAIST. Her main research focuses on the design and synthesis of nanoporous organic polymers for the environmental applications.



Sang Hyun Je received his MSc (2013) and PhD (2017) from Korea Advanced Institute of Science and Technology (KAIST), South Korea under the supervision of Prof. Ali Coskun. He obtained a postdoctoral fellowship from National Research Foundation of Korea and continued his research in the same group. His research focused on the molecular-level synthesis of porous organic polymers for lithium-sulfur battery, gas capture and conversion, and also catalysts.



Siddulu Naidu Talapaneni is a Research Associate at Global Innovative Center for Advanced Nanomaterials (GICAN), The University of Newcastle, Australia. He obtained MS in Chemistry from NIT-Warangal, India. He received PhD in 2012 from the National Institute for Materials Science (NIMS), Tsukuba in collaboration with Hokkaido University, Japan. He then worked as a postdoctoral researcher at the Laboratory of Catalysis and Spectrochemistry (LCS), ENSICAEN, France, Korea Advanced Institute of Science and Technology (KAIST), and Future Industries Institute (FII), University of South Australia, Australia. His research work mainly focuses on the design and development of nanoporous materials to tackle the energy and environmental issues.



Ali Coskun received his PhD degree in Chemistry from Middle East Technical University, Ankara, Turkey in 2007. He then joined to the laboratory of Prof. J. Fraser Stoddart as a postdoctoral research associate at Northwestern University, where he developed dynamic metal-organic frameworks, artificial molecular machines, organic radicals. He started his independent career at Korea Advanced Institute of Science and Technology as an assistant professor in 2012. In 2017, he moved to University Fribourg, Switzerland as an Associate Professor. He is currently developing porous organic polymers for CO₂ capture, separation and conversion and also supramolecular polymers for Li-ion batteries.



focus on POPs. A brief overview on the textural properties and water uptake behaviors for the samples discussed in this work is given in Table 1.

1.1 Assessing the Stability of desiccants in water

The hydrolytic stability of a sorbent is the first critical factor, which needs to be considered. The most representative methods for determining water stability of the sorbents include powder X-ray Diffraction (PXRD) analysis and nitrogen adsorption isotherms at 77 K before and after water vapour uptake measurements. However, PXRD is only useful in the crystalline materials such as MOFs, COFs and nitrogen adsorption isotherms in the most carbon- or silica-based porous materials generally do not show any significant change in their values, hence an appropriate method that is specific to the properties of each material should be used. Alternatively, the stability may be assessed by performing structural analyses such as nuclear magnetic resonance (NMR) spectroscopy and surface area analysis after immersing the adsorbent in water. More recently, it has also been proposed to expose sorbents to high-humidity and temperature conditions as a method to evaluate their stability. Critically, the most important requirement for such a stability measurement is that it needs to be performed under the environment in which the actual adsorbent would be used. For example, in a 'single cycle condition, i.e., an adsorbent for water-oil separation, the adsorbent may only be stable until the maximum adsorption capacity amount is reached, but in a continuous system such as air separation, flue gas or fuel purification, the structure and performance of the adsorbent must be maintained after several adsorption-regeneration cycles. Many studies try to replicate these conditions at a laboratory level, but it is rather difficult due to the large number of impurities (SO_x, NO_x, N₂, or dust) present in the actual gas mixtures. Therefore, when considering the hydrolytic stability of adsorbents, the physical stability and type of process must be considered along with the maximum adsorption capacities and cyclability.

1.2 Water vapour adsorption techniques

The porous sorbents could be categorized into three groups according to their pore sizes: i) macroporous (50 – 100 nm), ii) mesoporous (2 – 50 nm), and iii) microporous (<2 nm), and they can be further distinguished into six isotherm types based on their nitrogen adsorption isotherms. The detailed description of isotherm profiles will not be discussed in this review, however interested readers could reference to the review article on this topic.^[17] Here, we primarily focus on the adsorption isotherms in order to differentiate the hydrophobicity and the hydrophilicity of the adsorbent and how to use these isotherms when evaluating water uptake isotherms.

Hydrophilic adsorbents have naturally strong interactions with water molecules, typically zeolite and silica-based sorbents are classified as hydrophilic. Previously, these characteristics have been pointed out as demerits since they lower the adsorption efficiency of target gases such as CO₂ or CH₄ due to the competitive binding, but recently they become great advantages for moisture adsorption. Conversely, although most carbon materials have been known to be hydrophobic, in reality, some of these

REVIEW

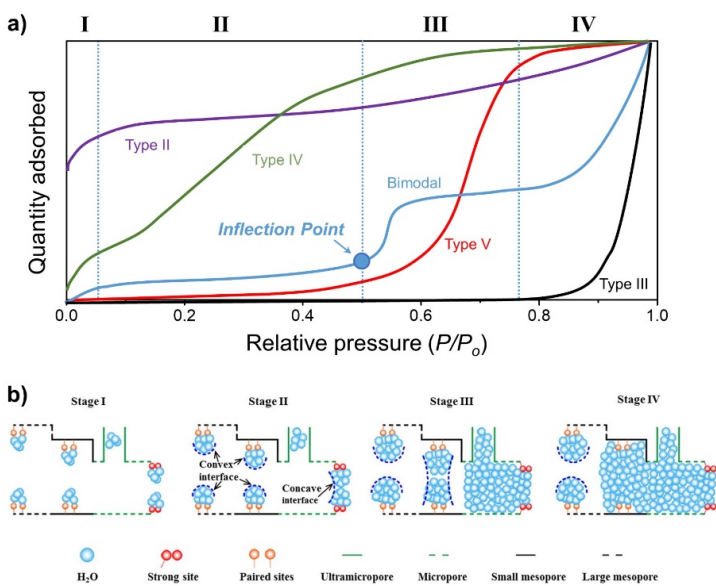


Figure 1. (a) Water vapour adsorption isotherm types according to the IUPAC classification. (b) Mechanism of water sorption in each stage. Reprinted from Ref [30].

materials could adsorb a large amount of water. From this phenomenon, it is assumed that the moisture adsorption is greatly influenced by the pore volume rather than the nature of the material. Then, how do we actually distinguish between hydrophilic and hydrophobic sorbents? The answer lies in their adsorption isotherms. The water vapour adsorption isotherms can be interpreted in the same way as the traditional gas adsorption isotherms at room temperature. For example, substances that exhibit rapid adsorption at low relative pressures could be considered as hydrophilic materials due to the strong interactions between water molecules and adsorbents. On the contrary, if the isotherm profile shows nearly no to little adsorption at low pressure region, the material would be classified as a hydrophobic sorbent. Namely, hydrophilicity is proportional to the slope of the graph at zero loading. The quantitative indexes were proposed by Anderson and Klinowski,^[18] Weitkamp,^[19] and Giaya.^[20]

Various methods to analyze the quantity of adsorbed water vapour amount have been developed. One of the methods is to measure the change in the weight of the sample at different temperatures. Vapour uptake capacity can be determined simply from the weight difference obtained at room temperature and high temperature ($\sim 400^\circ\text{C}$). Here, it is assumed that the adsorbed vapour is coming solely from the ambient air. However, when we use oven or thermogravimetric analysis (TGA) instruments, it could be hard to distinguish the types of gases and thus the obtained adsorption values could also include impurities or other adsorbed gases along with water. To account for this effect, degassed adsorbents can be exposed to a humid environment or water vapour during the measurement.

For an accurate uptake measurement, recording adsorption/desorption isotherms through a standard surface area analysis, i.e., Brunauer-Emmett-Teller (BET), is a typical method. In most cases, isotherm of the adsorbent is investigated at 298 K, and the adsorption amount is plotted as a function of the relative pressure ($P/P_0 = 0-1.0$ where P_0 is the saturated vapour pressure at given temperature) or relative humidity (RH = 0-100%). When

the relative pressure is close to 1, the maximum adsorption amount ($\text{cm}^3\text{H}_2\text{O} / \text{g}$ of sample) can be determined, which is highly related to pore volume, with the exception of superhydrophobic microporous solids, wherein the water adsorption mechanism is based on liquid water intrusion.^[21] In the case of mesoporous materials, capillary condensation occurs due to the bottleneck phenomenon, resulting in a difference in the adsorption-desorption curve, called 'hysteresis loop'. In addition, the relative pressure at which half of the total water capacity reached is also another comparable factor to evaluate the hydrophobicity of adsorbents. The units for water adsorption is generally represented as $\text{cm}^3 \text{g}^{-1}$ (volume of water adsorbed per gram of adsorbent), which can be converted to wt% (weight percent of water adsorbed per gram of adsorbent). The isosteric heat of adsorption at zero coverage (Q_{st}) is also a good indicator for the hydrophobicity/philicity of sorbents, which will directly effect the required regeneration temperature. The isosteric enthalpy of adsorption can be calculated from the Clausius-Clapeyron equation, given by

$$\Delta H = R \left(\frac{d(\ln P)}{d(-\frac{1}{T})} \right)_w \quad (\text{Eq. 1})$$

where ΔH , R , P , T , and w , represent the isosteric enthalpy of adsorption, universal gas constant, pressure, temperature, and vapor uptake, respectively.

IUPAC classifies isotherm types for adsorbents that are microporous (Type I), nonporous or macroporous (Type II, III, and VI), or mesoporous (Type IV and V). For water vapor sorption, Type I isotherms are observed for the strongest adsorbate-adsorbent interactions, which are commonly observed in strongly hydrophilic materials such as zeolites and some MOFs with open metal sites. The maximum loading typically lie at very low relative pressure regions. Type I isotherm is applicable for the water filling as a monolayer on the internal surface of the material. Type II isotherms also show a major adsorption in the low relative pressure region, but via multilayer adsorption on the internal surface of the material. The relatively high adsorbate-adsorbent interactions can be achieved by creating primary active centers. Type III isotherms do not show any identifiable monolayer formation and also the adsorbent-adsorbate interactions are relatively weak. This type of isotherm implies strong hydrophobicity of the pore space. Therefore, the water molecules are clustered around the most favourable sites on the surface of the material. Type IV isotherms are observed for materials that swell until the maximum point for site hydration is reached. The weak interaction between water and adsorbent is also observed for Type V isotherms. Type V isotherms are typically accompanied with a strong hysteresis loop, which is mainly observed for weakly hydrophobic mesoporous materials that undergo capillary condensation. Among these isotherms, most commonly observed for water uptake in activated carbon and porous organic polymers are Type II, III, IV, V and bimodal one as shown in Figure 1a. The adsorption mechanism at each stage is further described in Figure 1b. The stages I, II, III and IV represent progressive formation of water clusters, cluster growth and coalescence, micropore filling, and mesopore filling, respectively. In wider pores such as mesopores, adsorbates are required to

REVIEW

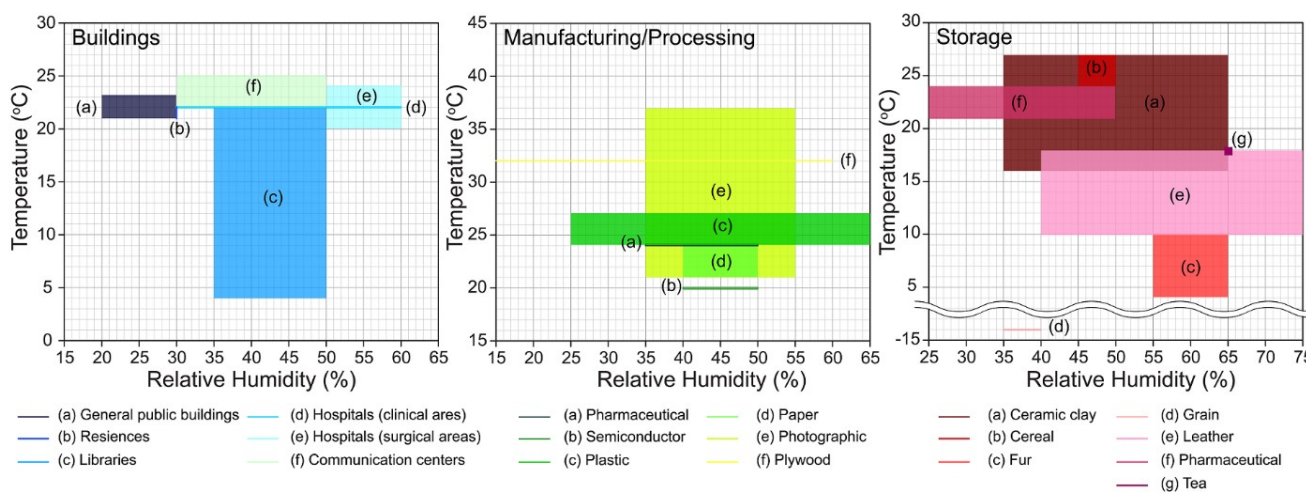


Figure 2. Plots of required temperature and relative humidity levels for different applications such as buildings, manufacturing or processing and storage.

form a bridge, which necessitates higher chemical potential. For materials with smaller pores such as micropores, the adsorption occurs preferentially in these pores.

1.3 Potential applications

Understanding the water adsorption behavior is of prime importance for the design of micro-and nanofluidic devices, water purification systems, steam regenerators, removal of contaminants from humid gas streams, desiccants, aqueous based efficient energy storage and conversion devices and electrocatalysts as well as in several essential applications such as batteries, supercapacitors, water splitting, hydrogen evolution and oxygen reduction/evolution reactions.^[22]

In addition, since water is present everywhere, controlling the humidity levels is significant in many industrial or household applications. For each application, the selection of a proper adsorbent will depend on the desirable temperature and humidity ranges as shown in Figure 2.^[23] For general public buildings such as airport terminals and office buildings, the comfortable temperature and humidity levels fall between 21–23 °C and 20–30% RH, respectively. For libraries, different humidity and temperature conditions are required depending on specific areas such as archival (35% RH), art storage (50% RH). Humidity control is essential in hospital buildings where the risk of infection is directly associated with human health. Humidity and temperature can also affect the quality of final products in manufacturing. Pharmaceutical products involving compressing and coating tablets, manufacturing ampules and packing medicines require temperature of 24 °C and humidity range between 35–50% RH. The assembly of semiconductors requires a specific temperature of 20 °C and humidity between 40–50% RH. The specific conditions are also required to maintain the product quality and freshness during storage. The required conditions for storing tea is 18 °C and 65% RH while grain storage requires lower temperature (-14 °C) and humidity (35–40% RH). In desert and arid regions where water scarcity is a serious issue, the day-time humidity is as low as ~10% with temperature of 30–40 °C and night-time humidity level is ~40% RH

with temperatures in the range of 15–25 °C. These listed applications are the examples where the water sorption is essential. The optimum water sorption is expected to be achieved by using ‘water favourable desiccants’ where hydrophilic desiccants could effectively adsorb atmospheric water.

One of the widely known industrial applications taking advantage of ‘water favourable desiccants’ is the desiccant driven air conditioning or refrigeration systems^[13d]. Unlike conventional refrigeration or air-conditioning systems, the desiccant driven systems do not involve hydrochlorofluorocarbon or hydrofluorocarbon refrigerants, which are considered as the main cause of ozone layer depletion. In an adsorption chiller, desiccant materials simply remove heat by evaporating liquid refrigerants such as water. The desired desiccants should possess high water uptake capacities and low regeneration temperatures. On the other hand, some applications require ‘non-water favourable adsorbents’ where hydrophobic or slightly hydrophilic adsorbents selectively adsorb target molecules against water. In these applications, water molecules generally act as contaminants as in post-combustion CO₂ capture.

POPs have been primarily studied in the context of carbon capture. The increasing CO₂ levels in the atmosphere originating from anthropogenic CO₂ emissions is a global concern owing to its major contribution to global warming. In this regard, the development of new materials for CO₂ capture and separation has received a great deal of attention. Naturally, several studies have focused on selective capture of CO₂ against water since flue gas mixture consist of N₂ (75–76%), CO₂ (15–16%) and H₂O (5–7%).^[24] Water can compete with CO₂ for adsorption sites, thus generally leading to a significant decrease in CO₂ uptake capacity. In this regard, ideal materials should have high thermal and hydrolytic stabilities as well as low affinity towards water vapour. It should, however, be noted that the simultaneous realization of hydrophobicity and CO₂-philicity is a challenging task and requires fundamental understanding of interaction of water and CO₂ molecules with the sorbent.

In addition to CO₂, the emission of volatile organic compounds (VOCs) have also increased from industrial processes and from domestic consumption. Though the amount of VOCs in the

REVIEW

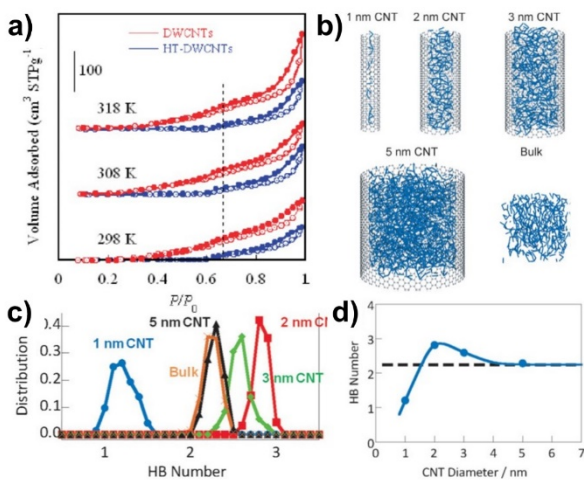


Figure 3. (a) Water adsorption isotherms of double walled carbon nanotubes (DWCNTs) and heat treated DWCNTs (HT-DWCNTs) at different temperatures. (b) HRMC simulations of hydrogen bonds of the water in the CNTs and bulk water. (c) Hydrogen bond numbers distribution of water molecules confined in the CNTs and bulk water. (d) Mean hydrogen bond number relative to the CNT diameter. The dashed line shows the hydrogen bond number in bulk water. Reprinted from Refs. [31] and [32], respectively.

atmosphere is lower compared to CO_2 , their life-time is substantially higher due to their high stability. Moreover, because of their high vapour pressures and low boiling points, VOCs can be emitted easily into the atmosphere, acting as air pollutants and toxic chemicals. For any sorption application, the adsorbent can be exposed to ambient air and the effectiveness of sorbents highly depend on the humidity of surrounding environment. For example, water clusters can form around the pore with active sites and block the adsorption of VOCs. Therefore, understanding the behavior of sorbents under humid conditions along with their affinity towards water is a critical task in order to improve their performance.

2. Water adsorption on zeolites and porous carbon materials

The water uptake in the nanoporous inorganic materials such as zeolites, zeo-type materials, mesoporous silica, and activated alumina has been considered as an important field of research because of their high adsorption capacity, high water selectivity at various concentrations and their usage in clean energy systems such as electric dehumidifiers, adsorption-driven heat exchangers and adsorption based heat pumps.^[13b] Unique hydrophilic properties coupled with favourable textural parameters such as high specific surface area and large pore volume render zeolites as attractive candidates for water adsorption in addition to their classical applications as ion-exchangers, molecular sieving and catalysis.^[14, 25] Aluminium containing microporous zeolites show type I water sorption isotherm indicating their high affinity towards water at low partial pressures.^[26] The selectivity and water uptake capacity of the zeolites depend highly on their framework type, pore structure, hetero-metals (Al, Ti, Sn, Zr etc) and their amounts, extra-framework cations and the distribution of silanol ($\text{Si}-\text{OH}$) groups which can interact with water molecules via hydrogen

bonding interaction.^[27] Evidently, three water molecules can adsorb onto a single silanol group. Mintova et al.^[14] have recently reviewed the water adsorption capacity of functional zeolite materials with respect to their hydrophilicity, porosity, chemical and structural features. Tatlier et al.^[28] have investigated the relationship between the theoretically accessible surface area and pore volume for water uptake, pore size, types of secondary building units and fractal dimensions of zeolites with their experimentally measured water uptake capacities.

The unique structural features of water molecules at the interface of hydrophobic carbon nanostructures led to complex structures due to the weak hydrogen bonding interactions compared to those of hydrophilic surfaces and bulk water.^[29] Hydrophobic nanoporous carbon materials with and without heteroatom doping have been widely studied for water adsorption at low pressures due to their high water adsorption capacity at low humidity, easy regeneration.^[30] The water adsorption isotherms of porous carbon materials show very low adsorption at $P/P_0 < 0.3$, which is characteristic of a hydrophobic surface, followed by a steep uptake at partial pressures between 0.3 and 1.0, depending on the type of porous structure and functional groups on the surface. Adsorption isotherms of water vapour in most of the porous carbon materials exhibit hysteresis loop with varying magnitudes and shapes depending on the pore aperture size of nanocarbons. In general, both adsorption and desorption isotherms of water in ultramicroporous carbon materials with pore sizes of below 0.7 nm follow the same profile, which results in the absence of hysteresis loop. Upon increase in the pore diameter of porous carbons (> 0.7 nm), hysteresis loop appears at partial pressures between 0.3 and 1.0.^[30]

Tao et al.^[31] demonstrated the water adsorption at 298, 308, and 318 K in the nanospaces of double walled carbon nanotubes (DWCNTs) and heat treated double walled carbon nanotubes (HT-DWCNTs) having surface areas of 510 and 350 $\text{m}^2 \text{ g}^{-1}$, respectively. Figure 3a shows the water adsorption isotherms measured for DWCNTs and HT-DWCNTs. The adsorption profiles are S-shaped suggesting two types of pore filling mechanism at two distinct adsorption steps of $P/P_0 = 0.3$ to 0.65 and for $P/P_0 = 0.65$ to ~1. The total pore volumes determined from the amount of adsorbed water at 318 K near saturation ($P/P_0 = 0.99$) for DWCNTs and HT-DWCNTs and were found to be 0.18 and $0.10 \text{ cm}^3 \text{ g}^{-1}$, respectively. Tomonori Ohba evaluated the formation of ice-like water clusters within the internal hydrophobic nanospace of CNTs with different inner diameters by using X-ray diffraction and molecular simulation analysis (Figure 3b).^[32] As depicted in Figure 3c and 3d, the water molecules in CNTs with a diameter of 1 nm had fewer hydrogen bonds than bulk water under ambient conditions. However, water molecules formed ice-like nanoclusters (0.8–3.4 nm) even under ambient conditions in CNTs with diameters of 2 and 3 nm because of strong intermolecular hydrogen bonding interactions. These results further indicate that 0.8 nm sized clusters are the fundamental units of water assemblies. Kaneko et al.^[31] demonstrated the dynamics of water adsorption in the carbon nanotubelites through the nanogates. They observed that the water molecules can enter into a nanohorn through a nanogate with a pore aperture of 0.5 nm on the wall of nanohorn. The kinetics of this phenomenon are much slower than the “normal” water adsorption, as the water nanoclusters have to form from the water nanochains in order to enter into the nanogates of carbon nanotubelites.^[33] Itami et al.^[34]

REVIEW

have explored the water adsorption properties of a new class of cycloparaphenylene ([12]CPP) carbonaceous porous solids with the uniform structure of 12 benzene molecules linked together. The adsorption/desorption isotherms of H_2O on [12]CPP has been measured at 298 K. Almost no adsorption was observed up to a relative pressure of $P/P_0 = 0.75$, then a sudden uptake occurred up to $P/P_0 = 1.0$. In the desorption process, no distinct hysteresis loop was observed. The water sorption isotherms indicate the adsorption of water molecules on small nonpolar pore surfaces.

Sullivan et al.^[22a] reported on the water uptake behaviors of Novoloid-based activated carbon fiber cloth (ACFC), Calgon BPL granular activated carbon (GAC), Calgon Zorflex™ activated carbon cloth, military ASZM-TEDA GAC, and electrospun activated carbon nanofibers (ACnF), respectively. They have concluded that the hydrogen treated porous Novoloid-based ACFC was more hydrophobic and exhibited the wide hysteresis loop compared to other tested activated carbons. Nakamura et al.^[35] also studied the effect of water adsorption with respect to the pore width (w) and equilibration time by using three pitch-based activated carbon fibers (ACFs) (AD'ALL Co.) and two kinds of phenol-resin-based ACFs (Kurare Co.). The adsorption isotherms of porous carbons with pore size of 1.1 nm shows a wide hysteresis loop and longer equilibration time ranging from 5 min to 16 h. The hydrophobic micropores of about 1 nm in width resulted in an indefinite adsorption hysteresis loop due to the metastable structure formation of water molecules on the adsorption branch. Importantly, water molecules cannot form the metastable structures on the pore walls in case the size of pores are less than the critical pore width of 0.6 nm, thus giving the hysteresis-free adsorption isotherms. Horikawa et al.^[36] studied the water adsorption hysteresis and their descending scanning curves on a highly graphitized thermal carbon black, CarboPack F, and a highly ordered mesoporous carbon, Hex, with hexagonal shaped pores. The hysteresis loop of water isotherm for Hex shows three steps; (1) adsorption of water molecules onto the functional groups presented at the junctions between adjacent basal planes of graphene layers, (2) water clusters grown around the functional groups, and (3) formation of larger clusters via bridging of adjacent small water clusters, followed by a complete pore filling of mesopores. Whereas, the hysteresis for CarboPack F spans over a wide range in the relative pressure range of 0 and 0.95. The hysteresis loop of CarboPack F extends over a very wide pressure range and the loop is larger at the point when the descend starts from a higher loading. Thommes et al.^[37] have studied the water adsorption in the representative ordered mesoporous materials such as CMK-1, CMK-3 and CMK-8 (mesoporous carbons prepared from MCM-48, SBA-15 and KIT-6 silica templates). The results deliberately suggest that the water adsorption mechanism in the hydrophobic mesoporous carbons is similar to the formation of water cluster mechanism suggested for the other carbon nanomaterials including carbon nanotubes and microporous carbon materials. Pore filling of water vapour into the nanospace of mesoporous carbons does not resemble the conventional condensation of wetting of fluids such as argon and nitrogen. However, the effect of temperature on the water evaporation in the highly ordered mesoporous carbons is similar to the capillary evaporation step observed for nitrogen and argon. These observations further prove that the depicted hysteresis is due to the differences in pore filling and emptying mechanisms.

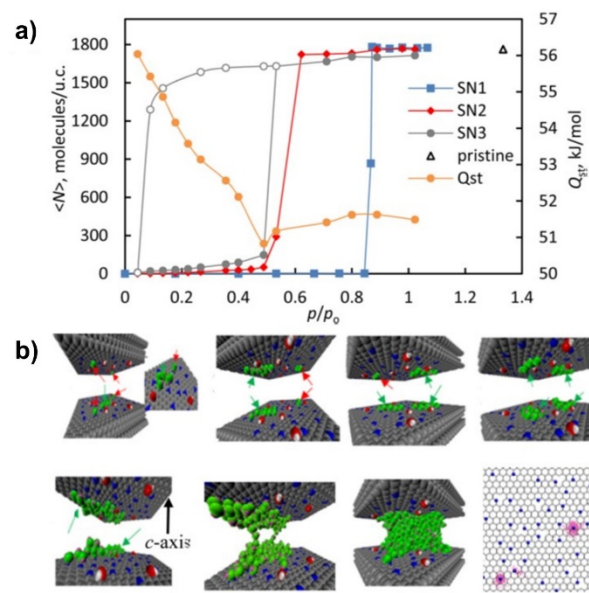


Figure 4. (a) Water vapor adsorption isotherms and the isosteric heat of adsorption in nitrogen doped carbon prototypes (b) A series of snapshots showing the equilibrium adsorption of water on nitrogen doped carbons at different relative pressures and the accumulation of water molecules on one side of the wall (Red arrows show the nucleation sites, green arrows correspond to 1D/2D water nanoclusters). Reprinted from Ref. [22].

Peter Lodewyckx investigated the kinetics of the adsorption of water vapour on activated carbon both theoretically and experimentally.^[38] The experimental data showed the existence of two types of adsorption mechanisms: a rather fast one and a very slow one. The slow kinetics could be explained by the formation of water nanochains in the ultramicropores (<0.7 nm) presented in the activated carbon, similar to the carbon nanotubelites. LeVan et al.^[39] and Do et al.^[40] have separately described a new equation for water adsorption equilibria on activated carbon. The model is consistent with Henry's law at low loading and it depicts the full range of isotherms with high accuracy using a small number of parameters. They have used this model for water adsorption equilibrium data on different types of carbons including ACF activated carbons, NC100, BPL, polymeric type E, PVDC, and UO3-1, which have large differences in surface area, surface chemical properties, and pore structure. The commonly observed hysteresis for these activated carbons is attributed to the slow relaxation of water clusters within the micropores.

Kumar et al.^[22b] have studied the water adsorption on nitrogen-doped carbons by using Monte Carlo simulations (Figure 4), wherein they used model carbon structures doped with graphitic-N and pyridinic-N. Figure 4b shows the adsorption of water molecules onto the N-doped carbon at different relative pressures of $P/P_0 = 0.044, 0.088, 0.177, 0.222$, and 0.266). In particular, at $P/P_0 = 0.044$ and 0.088 , they observed that the water molecules favorably adsorbed onto the N atoms (Figure 4i) through hydrogen bonding interactions on both sides of the pore wall. The authors have also showed the formation of 1D or 2D water nanoclusters over nitrogen atoms prior to the pore filling. In these materials, the graphitic nitrogen atoms retain the sp^2 planar structure of graphene. Weber et al.^[41] have studied the water

REVIEW

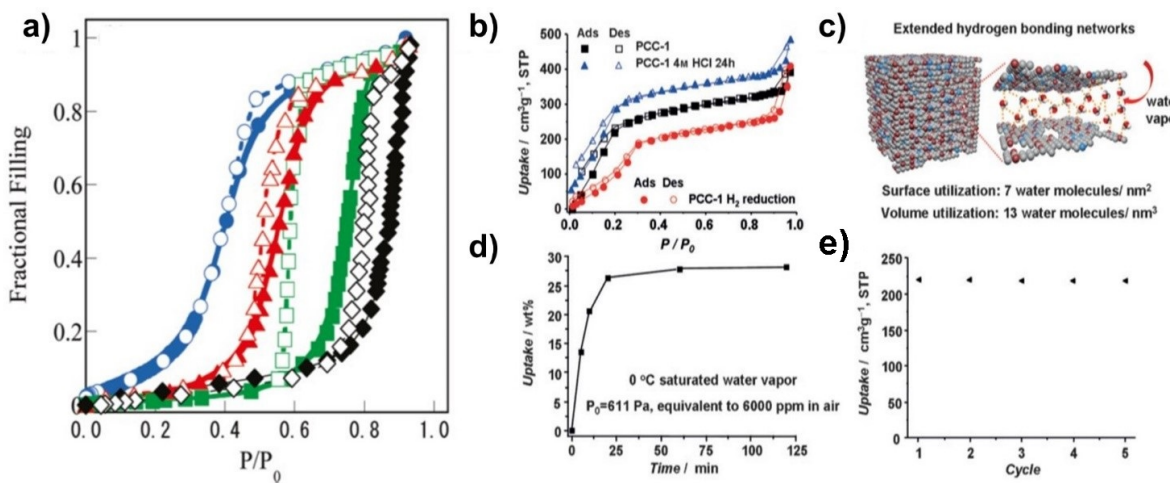


Figure 5. (a) Adsorption isotherms of water at 303 K for ACFs having average pore diameter of 0.7 (circles), 0.9 (triangles), 1.1 (squares), and 1.3 nm (diamonds) respectively. (b) Water adsorption performance of PCC-1 at 298 K, (c) schematic representation of low pressure water adsorption in the PCC carbon micropores via hydrogen bonding between water molecules as well as the water phase and carbon pore walls, respectively. (d-e) time dependent water sorption and cycling performance of PCC-1 carbon. Reprinted from Ref. [42] and [43], respectively.

vapour adsorption on microporous carbons and nitrogen enriched microporous carbons prepared through the carbonization of coconut shell and modified with formamide. All the carbon materials studied in this work showed type V water vapour adsorption isotherms indicating a weak gas–solid interactions especially at low relative pressure ($P/P_0 < 0.2$) range, wherein a very low uptake of water adsorption is observed. Steady state water cluster growth was observed, which was associated with the steep increase in water uptake at $P/P_0 = 0.4\text{--}0.7$ in the microporous carbons. The steeper part of the isotherm for the N-enriched sample is observed at a lower relative pressure range compared to undoped microporous carbon. Among the materials studied, nitrogen modified microporous carbons registered with high water uptake capacity of 1.46 mmol g⁻¹ at 298 K due to the effect of nitrogen enrichment, whereas unmodified microporous carbons showed water uptake capacity of 1.01 mmol g⁻¹ under identical experimental conditions. Ohba et al. [42] have used the pitch-based activated carbon fibers (ACFs; Ad'all Co.) having hydrophobic surface and a narrow pore size distribution for examining the mechanism of water vapour adsorption within the hydrophobic carbon micropores. This study was performed by the stabilization energy calculation and evaluation of the molecular assemblies of water formed during adsorption and desorption to clarify the physical reason for the occurrence of adsorption hysteresis in the case of hydrophobic micropores (pore width = 0.5–1.5 nm). Figure 5a shows the adsorption isotherms of water vapour at 303 K on hydrophobic activated carbon fibers with different average pore sizes. The adsorption of water vapour was not observed (Figure 5a) below a threshold pressure of water vapour adsorption, but significant adsorption occurs above this point for each sample. The threshold pressure increases with widening of average pore size in ACFs. The hysteresis loop size increases with an increase in average pore diameter of up to 1.1 nm. The adsorption and desorption pressures were shown to increase with widening of average pore diameter. The hysteresis of water adsorption indicates that adsorption or desorption (or both) path is in a metastable state.

Kaskel et al. [43] investigated the water uptake performance of porous carbon cuboids (PCCs) incorporating 14 wt% of nitrogen and 25 wt% of oxygen with unusual hydrophilic properties, over which the synergistic effects between surface heterogeneity and micropore architecture resulted in a water uptake capacity up to 9.82 mmol g⁻¹ at $P/P_0 = 0.2$ and 398 K (20% relative humidity or 6000 ppm) as shown in Figure 5b. The microporosity of the PCC was verified by type I nitrogen adsorption isotherm with a large uptake of N₂ at low relative pressures. The BET surface area, total pore volume and pore diameter of PCC were found to be 826 m² g⁻¹, 0.45 cm³ g⁻¹ and 7.6 Å, respectively. Remarkably, as shown in Figure 5c, it was calculated that 13 and 7 water molecules are trapped per nm³ of micropore volume and per nm² surface area of PCC-1, respectively, demonstrating the high efficiency of heterogenized microporosity as a “H₂O reservoir”. The water vapour uptake performance of PCCs outperformed all of the representative materials including commercial BPL activated carbon, carbon nanotubes, carbide derived carbon, nitrogen-doped carbon nanofiber, O-enriched porous carbons and synthetic carbons, benefitting from properties such as defined morphology, narrow pore size distribution, and high heterogeneity. The high water uptake capacity of PCC is explained on the basis of the presence of large number of hydrogen bonds between the doped carbon surface and water molecules which stabilizes the water phase by forming an extended intermolecular hydrogen bonding network. Sun et al. [44] engineered PCC material with tightly anchored cobalt/cobalt oxide nanoparticles (PCC-CoOx) through the post functionalization by the dispersion of CoCl₂ solution followed by pyrolysis. SEM and TEM images of PCC-CoOx revealed that the uniform CoO nanoparticles anchored onto hierarchical carbon cuboids that are randomly aggregated and overlapped with each other, with a rough surface and rich macropores even after Co/CoO loading, demonstrating its excellent structural stability. PCC-CoOx sample showed superior hydrophilic properties with a high water uptake capacity of 6.7 mmol g⁻¹ at a relative humidity of 20% and 25 °C. Hydrophilic ordered mesoporous carbon (HOMC) with an ordered

REVIEW

arrangement of uniformly sized mesopores was synthesized *via* a solvent-free nanocasting approach conducted in a planetary ball mill by using silica spheres as a structural template.^[45] Stemming from the synergistic effect of uniformly dispersed 34 wt% of heteroatoms (Nitrogen and Oxygen) and the highly ordered mesoporous structure and high specific surface area > 1000 m² g⁻¹, large pore volume >1.2 cm³ g⁻¹, the apparent water contact angle of the material is 0° – an unprecedented value for carbon materials. Hao et al.^[46] prepared hydrophilic, non-precious metal, nitrogen-doped carbon materials such as Fe/N_1/3.2, Fe/Cu/N_1.3/1.8, and Cu/N_1/4 with a surface composition contents of 74.7, 14.3, and 10.33% of C, N, and O, respectively. They all exhibited relatively good hydrophilic properties, with the water uptake capacities of 5.37, 5.38, and 5.96 mmol g⁻¹ at $P/P_0 = 0.3$ and 298 K for Fe/N_1/3.2, Fe/Cu/N_1.3/1.8, and Cu/N_1/4, respectively.

3. Tailored porous organic polymers as desiccants

3.1. Crystalline porous organic polymers as desiccants

3.1.1. Covalent Organic Frameworks (COFs)

COFs are crystalline polymers,^[4] composed of light elements (B, C, N, O, Si) linked together by strong covalent bonds. COFs offer high surface areas and structural tunability by simply varying the nature of monomeric units. These unique properties of COFs render them as an excellent choice of next-generation adsorbents. The most common COF formation reactions include boronate/boroxine (B–O), imine (C=N) linkages. Reversible nature of these reactions promotes the crystallinity of resulting frameworks. While this reversibility is essential for the crystallinity, it naturally renders the resulting frameworks moisture sensitive, which limits the application of these materials to dry gas capture,

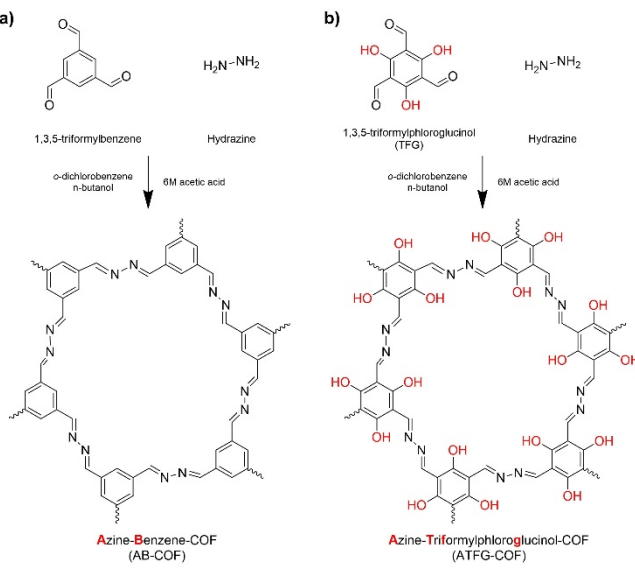


Figure 6. Schematic representation of the synthesis of AB-COF and ATFG-COF. Reprinted with permission from Ref. [47].

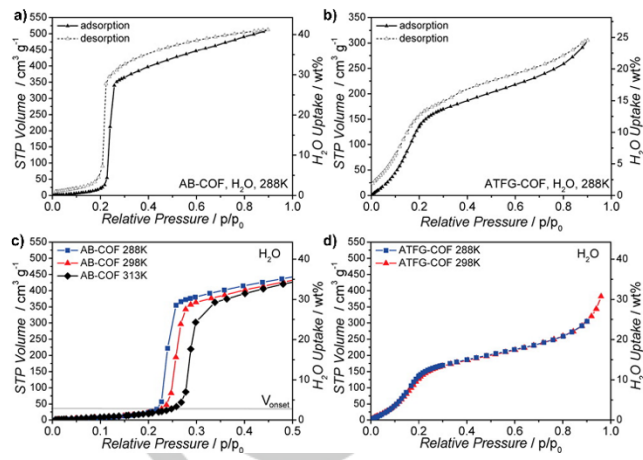


Figure 7. Water adsorption isotherms for (a) AB-COF and (b) ATFG-COF. Isotherms of (c) AB-COF, and (d) ATFG-COF at different temperatures. Reprinted from Ref. [47]

photovoltaics and energy storage. The synthesis of water stable COFs incorporating azine linkages, azine-benzene-COF (AB-COF) and azine-triformylphloroglucinol-COF (ATFG-COF), was reported by Lotsch and coworkers.^[47] AB-COF and ATFG-COF were synthesized by using 1,3,5-triformyl benzene and 1,3,5-triformyl-phloroglucinol as shown in Figure 6. The hydroxyl (-OH) group in ATFG-COF underwent tautomerization and the authors successfully proved the coexistence of two tautomeric forms. AB- and ATFG-COF exhibited high microporosity with BET surface areas of 1125 and 520 m² g⁻¹, and pore volumes of 0.47 and 0.50 cm³ g⁻¹, respectively. The volumetric water uptake performances of each azine COFs are shown in Figure 7. At $P/P_0=0.9$, maximum water uptake capacities for AB-COF and ATFG-COF were found to be 41 and 25 wt%, respectively, featuring S-shape profiles. In general, the amount of adsorbed water is proportional to the pore volume, however, ATFG-COF having higher pore volume with respect to AB-COF showed lower water uptake. This result might originate from the “ultramicroporous” nature of ATFG-COF with pore size less than 0.7 nm as water molecules are less likely to be adsorbed in these pores. It is, however, noteworthy to mention that the pore-wall of ATFG-COF is more hydrophilic due to the presence of polar functional groups such as nitrogen or oxygen and thus the adsorption amount increases rapidly at a low relative pressure ($P/P_0 = 0.2$).

Unlike porous carbons, a triazine-based COF with hydrophobic pore walls, trzn-COF, was shown to hardly adsorb any water.^[48] The trzn-COF exhibited a specific surface area of 408.5 m² g⁻¹ and a pore volume of 0.21 cm³ g⁻¹. The water uptake capacity was found to be only 4 wt% (2 mmol g⁻¹). The hydrophobicity of trzn-COF led to very weak interactions with water molecules. These results clearly demonstrate that the hydrophilic/hydrophobic nature of the pore walls greatly affects the water uptake capacity and serves as a critical guideline for the development of POPs to be used as water adsorbents.

Banerjee and coworkers reported a comprehensive study on the pore-wall modification of imine-linked COFs using 12 different organic linkers.^[49] 10 COF structures were synthesized along with C2 (amine) and C3 (aldehyde) combination resulting in hexagonal

REVIEW

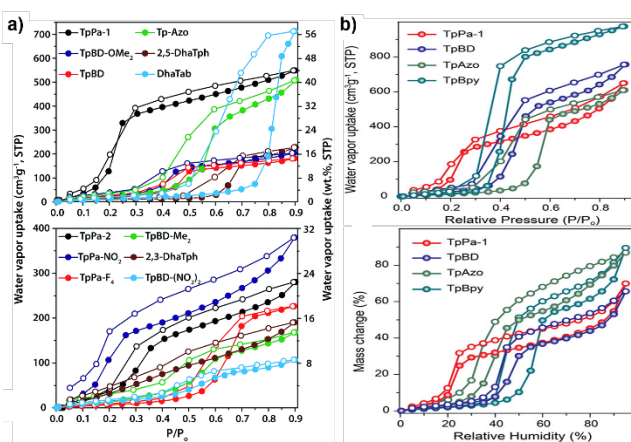


Figure 8. (a) Water sorption profiles of COFs using acetic acid as a catalyst. (b) Water uptake isotherms of COFs obtained using PTSA-H₂O as a catalyst. Reprinted from Ref [49] and [50], respectively.

structures (named as H-Series), and the other two structures were C2 (amine) with tetragonal C4 (amine-functionalized porphyrin) structure (T-Series). The amine-containing monomers were functionalized with -CH₃, -F, -NO₂, -OH, -N=N- groups and the trend of water uptake capacity was correlated to the nature of pore-walls. Firstly, the functionalization of COFs with hydrophobic groups such as -F, -NO₂, -CH₃ led to lower water vapour adsorption capacity (Figure 8). As expected, the highest adsorption capacity was obtained from hydrophilic functional groups, DhaTab (-OH group, 57 wt%) followed by TpPa-1 (-H group, 44 wt%) and Tp-azo (azo-linked, 41 wt%). TpPa-1 showed an abrupt increase in the water uptake at a low relative pressure range ($\sim P/P_0 = 0.3$).

Notably, the water uptake performance of TpPa-1 was superior to those of other carbon and MOF materials. In addition, 2,5-DhaTab with hydrophilic functional groups also showed a very high water uptake capacity of 17 wt%. 2,3-DhaTph and 2,5-DhaTph (T-Series) showed very little effect in water uptake due to the hydrophobic nature of porphyrin units in their backbone. The water adsorption-desorption cycle performances were investigated for the three COFs – namely, TpPa-1, TpPa-2 and Tp-Azo. These polymers showed excellent single-component water uptake isotherms in terms of adsorption capacity and working capacities. Over five cycles, they all showed stable adsorption-desorption performance and sustained their PXRD patterns, thus demonstrating the stability of the frameworks. Though these COFs synthesized using glacial acetic acid as a catalyst, later on, the same group reported a new synthetic strategy by using p-toluenesulfonic acid (PTSA-H₂O)^[50] as a catalyst, which improved the scalability and processability as well as morphology control over the final polymer using a suitable mold. For example, membrane, hollow tube, or a cylindrical shape could be obtained without using any binder or a crosslinking agent. More interestingly, the resulting polymers were found to be shape-persistent and did not lose their BET surface areas. Notably, the BET surface areas of the COFs synthesized using PTSA-H₂O as a catalyst were found to be 2 to 3 times higher than the ones obtained using acetic acid. These improved surface areas led to drastically improved water vapour uptake capacities. Accordingly, the water uptake capacities of TpPa-1 increased from 44 to 52

wt%, Tp-Azo from 41 to 49 wt%, and TpBD from 15 to 61 wt%. Furthermore, TpBpy containing bipyridine linkages exhibited water vapour uptake capacity of 78 wt%. Cycling performances of TpPa-1 and TpBD in a cylindrical shape were also performed up to four cycles, which showed stable cycling without any capacity loss.

3.1.2. Covalent triazine frameworks, CTFs

Covalent Triazine Frameworks (CTFs) are the subclass of porous organic polymers. CTFs have been applied to a variety of applications owing to their high nitrogen content, high surface area, stable structural properties, and porous structure. The first reported CTF by Thomas and Antonietti was synthesized under ionothermal reaction conditions using 1,4-dicyanobenzene and ZnCl₂ catalyst through the trimerization of cyano group (-CN).^[51] More recently, new synthetic strategies have been introduced to eliminate ZnCl₂ as a catalyst due to the difficulty of removing residual metals from micropores, these methods include strong acid,^[52] sulfur,^[53] P₂O₅,^[54] poly-condensation reaction,^[55] or monomer tuning.^[56] Another advantage of CTFs is their structural diversity through molecular-level design of monomers, enabling control over surface area, pore size, as well as hydrophobicity and hydrophilicity. CTFs can be obtained in both crystalline and amorphous forms depending on the reaction conditions.

In this review, we classify any porous organic polymer containing triazine units as CTF and discussed the water uptake performance of both crystalline and amorphous CTFs together in this section. Cyanate resins exhibit good thermal stability, permittivity and mechanical properties, but they are known for their low moisture adsorption characteristics. Wang et al.^[57] transformed cyanate resins into triazine-containing polymers through thermal-cyclotrimerization reaction. Each of the nitrile functionalized monomers – namely, tetrakis (4-cyanatophenyl) silane, tetrakis (4-cyanatobiphenyl) silane and tris (4-cyanatobiphenyl) amine – was subjected to thermal cyclotrimerization using nonylphenol as a catalysts to obtain

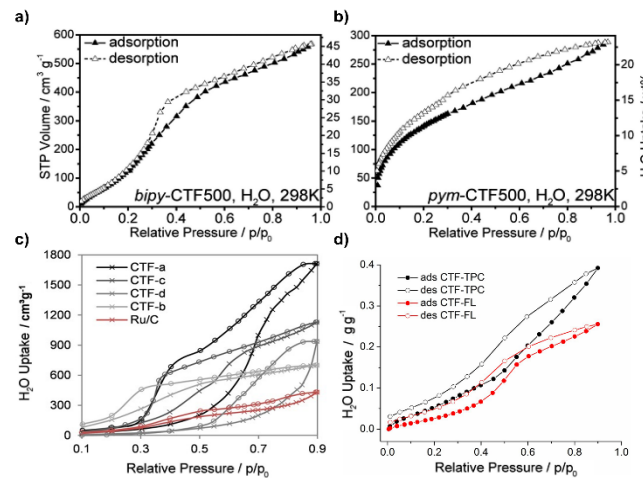


Figure 9. Water vapor adsorption/desorption isotherms of covalent triazine frameworks, (a-b) bipy-CTF-500, pym-CTF-500, (c) CTF-a to CTF-d, and (d) CTF-TPC/FL (closed symbols, adsorption; open symbols, desorption). Reprinted with permission from Ref. [58], [59], and [60], respectively.

REVIEW

crosslinked cyanate resin polymers (CE-1, CE-2, CE-3). The resin series (CE-1, CE-2, and CE-3) showed specific surface areas of 960, 588 and $540 \text{ m}^2 \text{ g}^{-1}$, and pore volumes of 0.97, 0.47 and $0.43 \text{ cm}^3 \text{ g}^{-1}$, respectively. CE-2 and CE-3 exhibited almost linear isotherms, an indication for the weak noncovalent interactions between water molecules and CE-2 and CE-3, thus pointing to the hydrophobic nature of pore-wall. The order of maximum water vapour uptake capacities at $P/P_0 = 0.9$ followed the pore volume, CE-1 > CE-2 > CE-3. In addition, CE-1 is considered to be more hydrophilic compared to both CE-2 and CE-3 due to its higher heteroatom (N, O) content.

The first attempt to use CTFs for water adsorption is reported by Lotsch group.^[58] They tested various CTFs for water adsorption. The CTFs were obtained using 1,4-dicyanobenzene (CTF-1), pyrimidine-2,5-dicarbonitrile (pym-CTF), 2,6-dimethylpyridine-3,5-dicarbonitrile (lut-CTF), and 2,2-bipyridine (bipy-CTF) in the presence of ZnCl_2 under ionothermal conditions. The reaction temperature was varied from 300 to 600 °C. While the low reaction temperatures (300–400 °C) led to the formation of crystalline CTFs, higher reaction temperatures (400–600 °C) led to partially carbonized, amorphous CTFs with significantly increased surface areas and porosity. Both bipy-CTF500, pym-CTF500 showed excellent performance in CO_2 uptake capacity and selectivity. These CTFs were also evaluated as water vapour adsorbents (Figure 9). While bipy-CTF500 showed a gradual increase in water uptake at low pressure, the profile of pym-CTF500 steeply increased at low pressure, which indicates its higher hydrophilicity. Water uptake capacities of 45 and 22 wt% were observed at $P/P_0 = 0.9$ for bipy-CTF500 and pym-CTF500, respectively. Around the same time, Palkovits and coworkers used 1,3-dicyanobenzene (1,3-DCB), 2,6-pyridinedicarbonitrile (2,6-DCP), 1,4-DCB and 4,4-biphenyldicarbonitrile monomers to synthesize CTF-a, CTF-b, CTF-c, and CTF-d, respectively.^[59] Though, the purpose of this study was to utilize the CTF backbone as a template for ruthenium catalysts in the oxidation of 5-hydroxymethylfurfural, the authors also carried out water adsorption experiments (Figure 9C) in order to probe the hydrophilicity of the CTF template. CTF-a to -d showed good affinity towards water vapour along with high water uptake capacities compared to the control sample, Ru/C. The highest vapour adsorption capacity was observed from CTF-a due to the fact that it has the highest pore volume among all the CTFs tested. One way to quantify the hydrophilicity is the degree of pore filling (DPF) value, which is the ratio of total pore volume to water adsorption capacity at $P/P_0 = 0.9$. Compared to other CTFs, CTF-b showed the highest DPF value (87.5) by virtue of its high nitrogen content, whereas CTF-d with high carbon content showed only 28.5, which indicates its hydrophobicity. This result is also further confirmed by comparing the water uptake capacities at low relative pressures. Except CTF-d, all the CTFs showed high water vapour uptakes below $P/P_0 = 0.3$, at which point the hydrophilicity of the framework becomes a very important parameter.

As mentioned above, though most of the CTFs are synthesized through the trimerization reaction using various catalysts, there are also reports on the synthesis of CTFs via Friedel-Crafts reaction using cyanuric chloride, AlCl_3 , and FeCl_3 as catalysts to reduce the synthesis temperature and avoid functional group limitations (cyano group). Janiak and coworkers synthesized CTF-TPC and CTF-FL by using tryptcene (TPC) and fluorenone

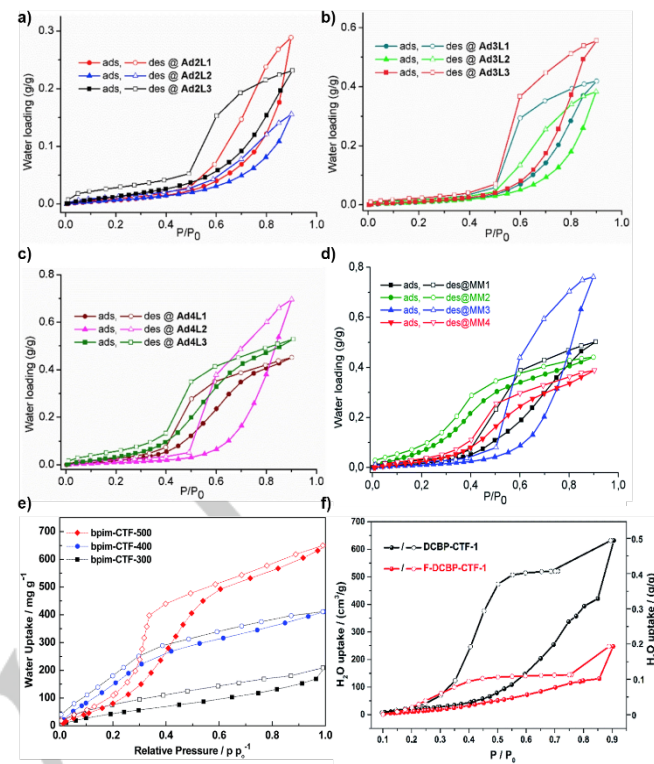


Figure 10. Adsorption isotherms (closed symbols) and desorption isotherms (open symbols) of water vapor for (a) Ad2 series, (b) Ad3 series, (c) Ad4 series, (d) MM series, (e) bpim-CTF series, and (f) F-DCBP-CTF. Reprinted with the permission from Ref. [61], [63], and [64].

(FL) as monomers, respectively, which are widely used as building blocks for the preparation of POPs.^[60] Both polymers were found to be completely amorphous, which is common for the kinetically controlled polymerization reactions. The surface areas of CTF-TPC and CTF-FL were found to be 1668 and $773 \text{ m}^2 \text{ g}^{-1}$ with total pore volumes of 0.93 and $0.39 \text{ cm}^3 \text{ g}^{-1}$, respectively. Abnormally high oxygen ratio was observed for both polymers in the elemental analysis, which prompted the authors to hypothesize that the materials are hygroscopic. In order to demonstrate this, the Karl-Fischer titration (KFT) method and the general vapour sorption isotherm were used. KFT analysis showed that degassed polymer can adsorb approximately 10–13 wt% of water vapour from ambient air. In contrast, vapour adsorption isotherms indicate that CTF-TPC and CTF-FL can adsorb up to 34 wt% and 21 wt% of water vapour at a relative pressure of 0.9, respectively.

Later on, Janiak and coworkers employed mixed-linker approach for the synthesis of CTFs through conventional ZnCl_2 catalysts.^[61] The mixed-linker approach is a widely used method to prepare COFs or POPs to form pores with different sizes depending on the length of the linker. As shown in Figure 10, nine different CTFs were synthesized with the combination of three different adamantane cores (Ad₂–Ad₄) and cyano linkers (L₁–L₃).^[61a] In a separate study, the authors also used tetraphenylethylene as the main core and reacted it with four different cyano linkers (M1 to M4) in the presence of ZnCl_2 forming MM'-CTF polymers.^[61b] As the synthesis and analysis methods are similar except the main core unit, we will discuss these results together. As listed in Table

REVIEW

1, all the CTFs based on this two-linker approach showed excellent surface areas and pore volumes. For example, Ad₄L₂-CTF showed the surface area and pore volume values of 1885 m² g⁻¹ and 1.52 cm³ g⁻¹, respectively, whereas, in the MM series, MM3 (400) showed surface area and pore volume of 1884 m² g⁻¹ and 1.52 cm³ g⁻¹, respectively. Polymers synthesized above 400°C were excluded due to the partial carbonization. The water adsorption isotherm of each polymer is depicted in Figure 10a-c. All the Ad and MM series showed drastically increased water uptake values at high relative pressures compared to lower relative pressures mainly due to their hydrophobicity. Hence, the water adsorption occurred primarily through pore condensation. Among them, pore-wall of MM2 in MM series, incorporating tetrafluorophthalonitrile as a linker, is expected to be highly hydrophobic owing to the presence of fluorine atoms. However, MM2 showed much higher adsorption capacity at a lower relative pressure compared to other polymers as shown in Figure 10d. The authors explained this phenomenon by the capillary condensation effect within the micropores of MM2 as well as the hydrogen bonding interactions. Though it is common to explain the difference of adsorption at low relative pressures simply by hydrophobicity or hydrophilicity of the pores, it is rather difficult to exclude the effects originating from pore-volume, pore-size distribution, or other physical properties of the POPs. The above-mentioned experiments demonstrate that POPs exhibit a certain amount of water vapour adsorption at low relative pressures from ambient air. Coskun and coworkers^[62] also reported a similar behavior for the charged CTFs, for which the TGA analysis revealed significant mass loss at the elevated temperatures (< 150°C). The hydrophilic nature of cationic CTF were also shown by Yoon and coworkers for CTFs incorporating imidazolium ions, bpim-CTF.^[63] Hygroscopic nature of bpim-CTF is verified from TGA analysis with about 13 wt% weight loss in the temperature range of 100-120 °C, which could indicate the uptake of atmospheric moisture along with residual solvents. Notably, the water adsorption-desorption isotherms illustrate significant increase in water uptake with increasing polymerization temperature. This result can be explained by increasing pore volume (N/D, 0.34, 0.75 cm³ g⁻¹ for bpim-CTF-300, CTF-400, CTF-500, respectively) with rising reaction temperature. It is, however, important to note that at low relative pressures below 0.3, bpim-CTF-400 showed the highest water uptake capacity followed by bpim-CTF-500 (Figure 10e). This result can be explained by the significant loss of nitrogen atoms at 500 °C and the consequent decrease in hydrophilicity.

Very recently, Van Der Voort and coworkers synthesized fluorine substituted CTF, F-DCBP under ionothermal reaction conditions by reacting 2,2,3,3,5,5,6,6-octafluoro-4,4-biphenyldicarbonitrile (F-DCBP) in the presence of ZnCl₂ catalyst.^[64] Fluorine atoms are known to undergo partial dehydrofluorination and vaporize in the form of carbon-fluorine gas at elevated temperatures. DCBP-CTF synthesized from 4,4-biphenyldicarbonitrile (without any fluorine atoms) was used as a control sample. In good agreement with the previously reported CTFs, the specific surface area of F-DCBP was found to largely depend on the ZnCl₂ ratio and the reaction temperature. F-DCBP-CTF-1 with 5 equiv. of ZnCl₂ exhibited a surface area of 1574 m² g⁻¹, whereas F-DCBP-CTF-2 with 10 equiv. showed surface area of 1126 m² g⁻¹. However, an opposite trend was observed in the pore volumes. F-DCBP-CTF-2 showed a slightly higher pore

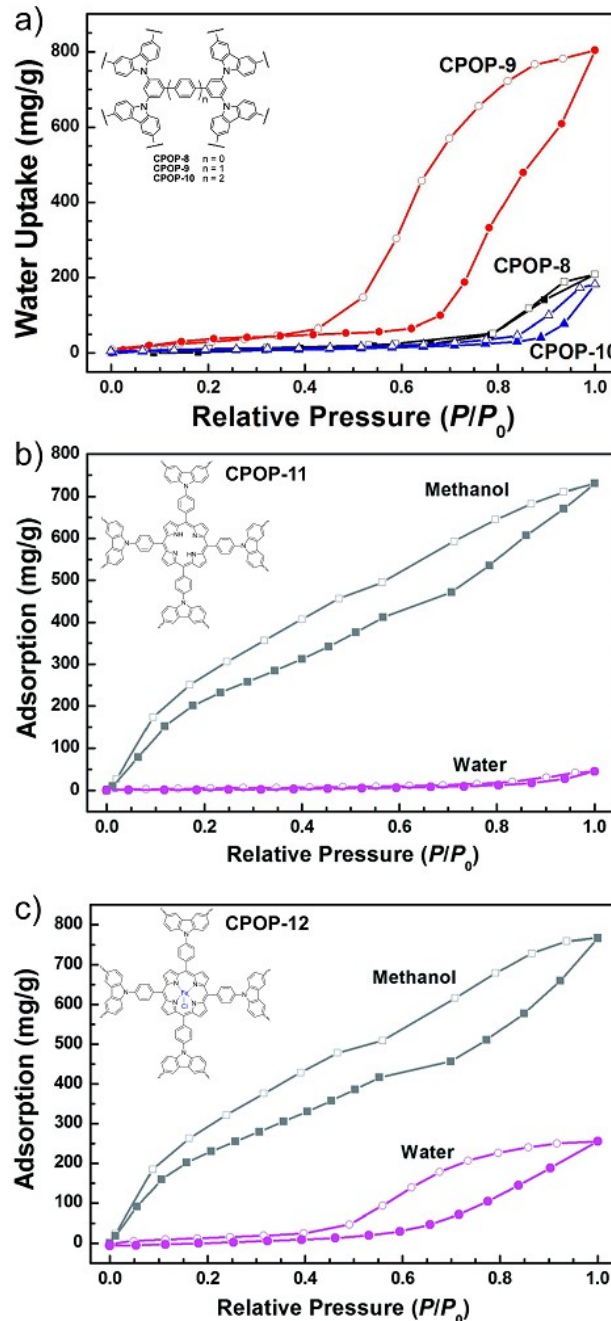


Figure 11. Adsorption (closed symbols) and desorption isotherms (open symbols) of water and methanol for (a) CPOP-8, CPOP-9, CPOP-10, (b) CPOP-11 and (c) CPOP-12. Reprinted with permission from Ref. [65], [66].

volume of 1.56 cm³ g⁻¹ compared to F-DCBP-CTF-1, 1.50 cm³ g⁻¹. The control polymers, DCBP-CTF-1, and DCBP-CTF-2 exhibited surface areas of 2437 and 2036 m² g⁻¹ along with the pore volumes of 1.48 and 2.26 cm³ g⁻¹, respectively. Elemental analysis revealed substantially lower fluorine contents for both F-DCBP-CTF-1 (4.2 wt%) and F-DCBP-CTF-2 (3.13 wt%) compared to the theoretical value of 43 wt%. The authors performed water vapour sorption measurements to investigate the effect of such a small amount of fluorine on the pore-walls.

REVIEW

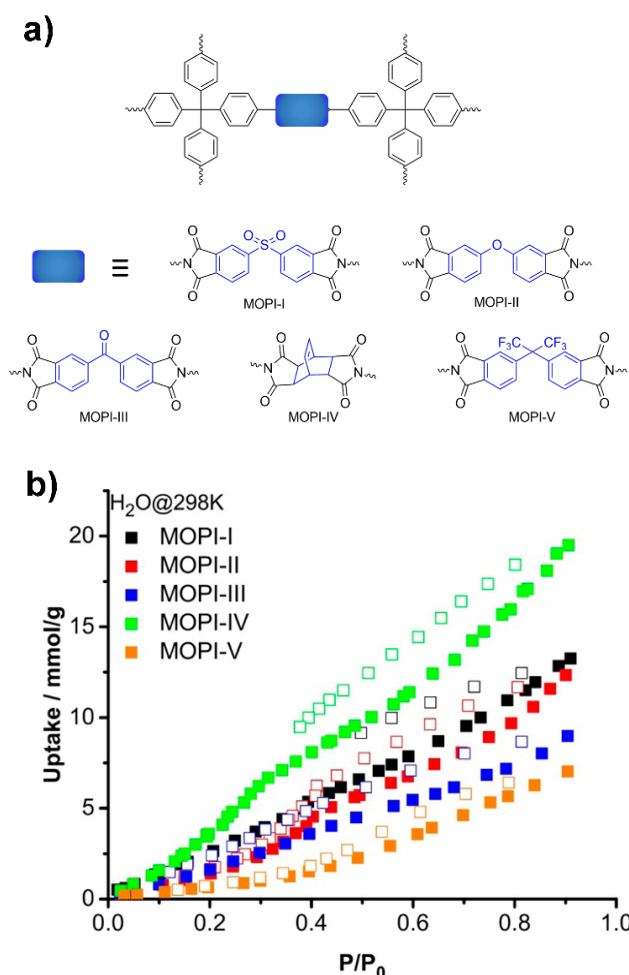


Figure 12. (a) Representation of MOPIs. (b) Adsorption (closed symbols) and desorption isotherms (open symbols) of water vapours for MOPIs. Reprinted with permission from Ref. [73]

The authors were able to show (Figure 10f) that slightly hydrophobic F-DCBP-CTF-1 showed much lower water vapor uptake capacities compared to DCBP-CTF-1 in the entire pressure range. Considering similar pore volume of these polymers ($1.48 \text{ vs } 1.50 \text{ cm}^3 \text{ g}^{-1}$) and mesoporosity of F-DCBP-CTF-1, a large difference in the adsorption capacity indicates that the C-F bond impeded the adsorption of water molecules in the micropores.

3.2. Amorphous porous organic polymers as desiccants

POPs have attracted much attention in recent years owing to their controllable surface area, permanent porosity, wide range of available synthetic routes and building blocks and most importantly, high moisture and thermal stability. These polymers were found to be mostly amorphous due to the kinetically controlled reaction conditions. POPs have been extensively studied in the gas capture and separation applications targeting CO_2 , H_2 , toxic gases, and recently water capture. However, it should be mentioned that the application of POPs in the context of water capture is still in its infancy, and further research efforts are expected in the coming years considering the importance of

this particular research area. In the following section, we summarized POPs tested for water sorption and the polymers were categorized based on their hydrophobic/hydrophilic nature. More specifically, hydrophobic adsorbents include polymers that primarily focus on the adsorption of gases against moisture, thus showing little to no affinity towards water molecules, whereas hydrophilic POPs are the ones reported mainly for water sorption applications.

3.2.1. Water unfavourable POPs

3.2.1.1. Single-component water vapour sorption

Han and coworkers synthesized a series of porous conjugated polycarbazoles^[65] (CPOP-8, CPOP-9, CPOP-10) by varying the number of phenyl rings in the monomers. Among all the CPOPs, CPOP-9 showed the highest surface area of $2440 \text{ m}^2 \text{ g}^{-1}$ and exhibited a predominantly mesoporous structure with pore size in range of 2.5-5.0 nm. Despite of its hydrophobicity, CPOP-9 showed (Figure 11a) high moisture uptake up to 64.6 wt% at $P/P_0 = 0.99$, consistent with its high pore volume ($2.04 \text{ cm}^3 \text{ g}^{-1}$). The pore volumes were found to be lower for CPOP-8 ($1.71 \text{ cm}^3 \text{ g}^{-1}$) and CPOP-10 ($0.76 \text{ cm}^3 \text{ g}^{-1}$), which in turn, resulted in much lower water uptake capacities of 16.7 and 13.6 wt%, respectively. The water adsorption isotherms of CPOP-8 and 10 showed a single step adsorption at $P/P_0 = 0.7$, which could be attributed to physisorption, swelling, and capillary condensation within the pore walls of the mesopores. A wide hysteresis loop in the case of CPOP-9 point to a different mechanism, that is adsorption/pore filling and desorption within hydrophobic materials. The water uptake in CPOP-9 is only observed at high relative pressures.

In addition, Han et al.^[66] also reported the synthesis of porous conjugated polymers (CPOP-11 and CPOP-12) incorporating porphyrin or Fe(II)-porphyrin moieties for the adsorption of organic vapours such as toluene and methanol. Both CPOPs showed much higher uptake values towards toluene and methanol compared to water, as shown in Figure 11b and c. Toluene adsorption isotherms present a gradual rise in adsorption until the material reaches saturation at 96 wt% for CPOP-11 and 119.2 wt% for CPOP-12. The good sorption capacity towards toluene is attributed to high porosity, complete organic nature and affinity to the guest molecules through $\pi-\pi$ and C-H/ π interactions. Moreover, CPOP-12 featuring a Fe(II)-porphyrin complex is relatively electron deficient, thus further increasing the affinity towards relatively electron-rich toluene molecules. For methanol sorption, CPOPs also present a gradual rise, which reaches up to 73.0 wt% for CPOP-11 and 76.6 wt% for CPOP-12 at the saturated vapour pressure of methanol. With respect to the sorption of organic vapours, water vapour adsorption showed much decreased values. The water sorption of CPOP-11 present little to no uptake until relative pressure of 0.8 (Figure 11b), which saturates at 4.6 wt%. The hydrophobic nature of CPOP-11 allows the extraction of methanol vapour under humid conditions. In contrast, CPOP-12 showed much higher water uptake capacity of 25.5 wt%, which is attributed to the increased hydrophilicity due to the presence of Fe(II)-porphyrin complex. The iron-porphyrin complex also showed a desorption hysteresis at $P/P_0 = 0.5-1.0$ presumably due to the interactions between water molecules and the metal centers.

REVIEW

Wang et al.^[67] reported the synthesis of microporous poly(Schiff base), PSN-3, in which each tetraphenyladamantane moiety is connected by aldimine functionalities through condensation reaction between formyl and amino groups. The nitrogen sorption analysis of PSN-3 showed the BET surface area of 865 m² g⁻¹ with the presence of micropores centered at about 0.60 nm as well as mesopores in a range of 2 to 30 nm. Due to its high porosity, PSN-3 presents potential for adsorption of benzene (80.5 wt% at $P/P_0 = 0.9$) and cyclohexane (63.7 wt% at $P/P_0 = 0.9$). However, the water sorption presents type III isotherm with maximum uptake of only 6.4 wt%. Wang et al.^[68] developed microporous polyimides that incorporate tetraphenylmethane and different linkers, namely, (hexafluoroisopropylidene)diphenyl (MPI-6FA), benzophenone (MPI-BPA) and biphenyl (MPI-BTA). Compared to non-fluorinated polymers, the fluorinated MPI-6FA showed higher BET surface area (781 m² g⁻¹), micropore surface area (473 m² g⁻¹) and micropore volume (0.22 cm³ g⁻¹). Despite of its high surface area and micropore volume, the water vapour uptake capacity of MPI-6FA was found to be smaller compared to other MPIs. The water sorption isotherm of MPI-6FA is found to be type III with a water uptake capacity of only 8.5 wt% at a relative pressure of 0.8. The convex-shaped isotherm presents hydrophobicity of MPI-6FA due to the presence of trifluoromethyl groups, which can effectively reduce the interaction between water molecules and the pore walls. The presence of hydrophobic fluorine atoms significantly alters water uptake properties, thus clearly showing the impact of hydrophobicity of microporous networks. Clearly, the type of functional groups is a significant factor in determining the degree of hydrophobicity within POPs. Provided that the polymers possess similar degree of hydrophobicity, the higher pore volume leads to increased water uptake capacity.

3.2.1.2. Multi-component vapour sorption

In the flue gas mixture, water is the third major component by volumetric concentration. Due to the presence of water, porous materials experience difficulty in selectively capturing CO₂ due to the competitive binding, which generally results in a decreased CO₂ uptake capacity as well as an inferior long-term stability. Though most of the porous materials lose their CO₂ uptake capacity, amine-doped porous organic polymers showed improved affinities. For example, Hamouz et al.^[69] reported an amine-rich crosslinked porous organic polymer (KFUPM-1) and performed breakthrough measurements to separate CO₂ from N₂ gas. First, the long term stability of KFUPM-1 is investigated through a multicycle continuous water uptake test at 313 K and RH = 76%. Up to 20 cycles, the material retained its water uptake properties, which indicates a good water stability within the given cycle range. For breakthrough experiments, the bed is packed with activated KFUPM-1 powder and subjected to a gas mixture containing CO₂ and N₂ (20 : 80 v/v) under dry or wet (RH = 91%) conditions. Under both conditions, KFUPM-1 selectively captured CO₂ while N₂ passes through the material. The longer CO₂ retention time is shown under humid conditions because KFUPM-1 adsorbs ~33.5 wt% water at 91% RH, which leads to stronger interactions with CO₂.

Hupp et al.^[70] presented a diimide-based porous organic polymer (NU-POP-1) for the capture of toxic industrial chemicals such as octane, ammonia, CNCl and SO₂. Since adsorbed water can alter the effectiveness of the sorbent, the performance of NU-

POP-1 is compared under dry and humid conditions. First, in single-component water uptake experiment, NU-POP-1 showed gravimetric water uptake capacity of ~22.5 wt% at RH=90%. In the entire humidity region, NU-POP-1 showed continuous increase in water uptake, which was attributed to its hydrophilicity originating from oxygen and nitrogen sites on the naphthalene diimide linkers. For binary micro-breakthrough experiments, the bed is filled with activated NU-POP-1 and subjected to one of chemicals such as octane, ammonia, CNCl and SO₂ under dry or wet (RH = 80%) conditions. Under dry conditions, NU-POP-1 showed high uptake capacities, whereas under humid conditions, the material yields elongated curves due to competitive adsorption of organic vapours and water.

3.2.2 Water favourable POPs

POPs are extremely stable under humid conditions, which renders them as excellent candidates for water capture applications. Hydrophilic POPs can be obtained by the incorporation of various heteroatoms (i.e., O, B, N, P, S) either as functional groups or bridging groups which can positively contribute to the interactions with water molecules.

In 2014, Kaskel et al.^[71] reported a series of 2D porous organic polymers OCF-1, DUT-92 and DUT-93 in the order of increasing number of phenyl moieties and also their derivatives with different functionalities such as NO₂ and NH₂ for DUT-92 and DUT-93. Interestingly, at low relative pressures, the water uptake properties of these polymers depended mainly on the interaction between water molecules and functional groups rather than the surface area and pore volume. The nitrogen adsorption isotherm of OCF-1, DUT-92 and DUT-93 showed high pore volumes above 1.02 cm³ g⁻¹ determined at a relative pressure of 0.97. However, the water sorption isotherms showed significantly low uptake at the low pressure region, indicating type III isotherm. This result was attributed to the highly hydrophobic nature of the porous networks. With increasing number of phenyl moieties, the polymers exhibited a decrease in their surface area and higher hydrophobicity. Similarly, Type III water adsorption isotherm is also observed for the polymers with nitro-functionalities accompanied by a small increase in the slope below $P/P_0 = 0.2$ pointing to a slightly polar surface due to the nitro groups. Furthermore, the degree of pore filling increases by 30-60% from non-functionalized polymers DUT-92 and DUT-93 to nitro-functionalized DUT-92(NO₂) and DUT-93(NO₂). On the other hand, amine-functionalized DUTs showed water uptake starting at partial pressures below $P/P_0 = 0.1$, indicating a more polar surface created by the amine groups. The water uptake capacity achieved with DUT-92(NH₂) was 24.5 wt% at $P/P_0 = 0.9$, which is much higher compared to the unfunctionalized DUT-92 with uptake capacity of only 8.0 wt% at $P/P_0 = 0.9$.

Senker et al.^[72] reported on the synthesis of porous imine-linked networks - namely, PIN1 and PIN2 - incorporating triazine moieties using DMSO as a solvent. Interestingly, when using DMSO as a solvent, the decomposition of DMSO at high temperatures led to the protonation of imine groups, thus forming ion pairs between C=NH⁺ - anionic decomposition products of DMSO. The presence of ionic functional groups rendered PIN1 and PIN2 highly polar and hydrophilic. In addition, from IAST calculation, PINs presented high selectivity towards H₂O over CO₂ (79.1 for PIN1 and 79.6 for PIN2) at 298 K. In comparison, PIN1

REVIEW

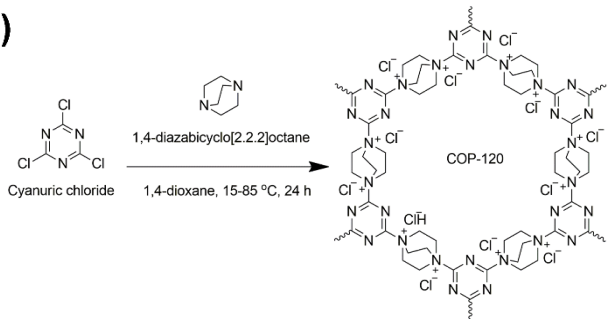
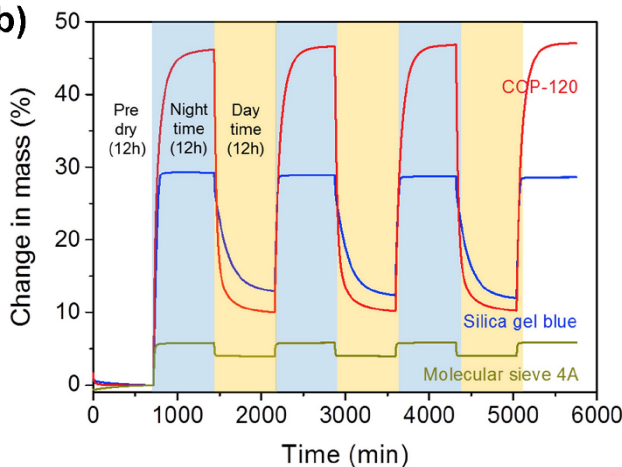
a)**b)**

Figure 13. (a) Schematic representation of COP-120. (b) Dynamic vapor sorption cycles measured at 25 °C for COP-120 and commercial desiccants such as silica blue and molecular sieve 4Å. The day and night time conditions are controlled by changing relative humidity between RH 30% (day) and RH 80% (night). Reprinted with permission from Ref. [74].

and 2 synthesized in DMF resulted in the formation of neutral polymers, which, in turn, led to much lower water uptake capacity (5.4 wt% at RH=90%) and also low selectivity (27.4) towards H₂O.

Apart from imine-linked porous networks, Senker et al.^[73] also reported a series of microporous organic polyimides (Figure 12a) that incorporate a range of bridging groups including diphenylsulfone (MOPI-I), diphenylether (MOPI-II), benzophenone (MOPI-III), bicyclic[2,2,2]oct-7-en (MOPI-IV), and hexafluoro-2,2-diphenylpropane (MOPI-V). All of the water sorption isotherms (Figure 12b) showed a gradual rise throughout the entire relative pressure range, indicating that the sorbents contain hydrophilic sites. However, the degree of hydrophilicity differs depending on the polarity of the bridging groups, which is verified by the water sorption experiments. In agreement with the previous work by Kaskel et al.^[71], the water sorption depends more on the interaction with functional groups rather than the surface area and pore volume. MOPI-IV incorporating bicyclooctene moiety showed the highest water uptake capacity of 34.4 wt% at $P/P_0 = 0.9$. MOPI-V with hexafluoro-functionalities presented the lowest water uptake capacity of 12.5 wt%, $P/P_0 = 0.9$ while exhibiting the highest surface area. The uptake capacities at RH = 90% follow the order of bicyclo[2,2,2]oct-7-en > diphenylsulfone > diphenylether > benzophenone > hexafluoro-2,2-diphenylpropane in agreement with the decreasing hydrophilicity of the frameworks.

In 2017, Yavuz et al.^[74] synthesized a hygroscopic POP through the polymerization reaction between cyanuric chloride and 1,4-diazabicyclo[2.2.2]octane (Figure 13a). The resulting charged POP, named COP-120, incorporates quaternary ammonium linkages. The hygroscopic properties induced by the charged centers led to a volumetric water uptake capacity as high as 44.9 wt% at $P/P_0 = 0.9$. In the moisture uptake cycles (Figure 13b), the activated COP-120 was subjected to a humidified gas flow with relative humidity according to day (RH = 30%) and night (RH = 80%) time conditions. The temperature is maintained at 25 °C for

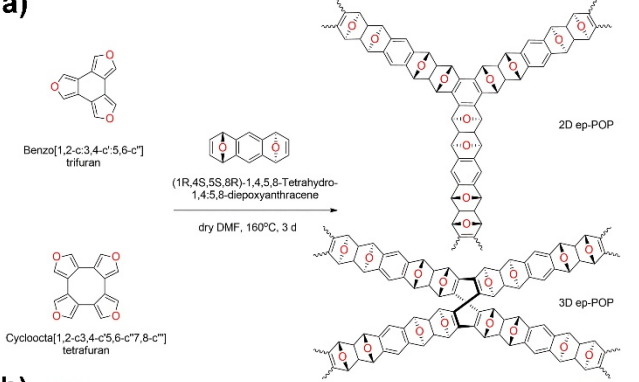
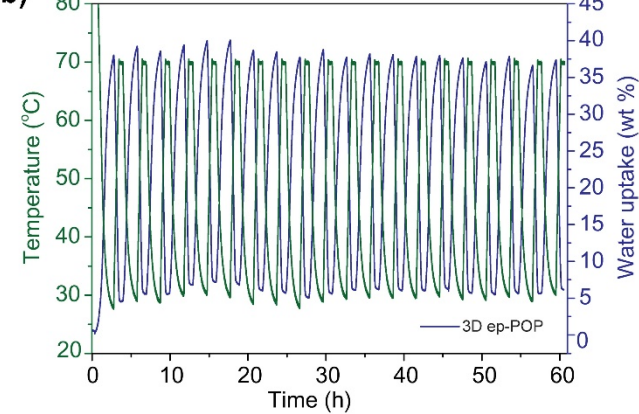
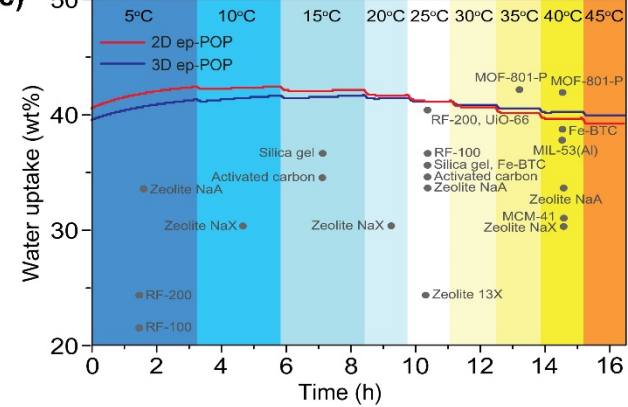
a)**b)****c)**

Figure 14. (a) Schematic representation of ep-POPs. (b) Dynamic vapor sorption cycles measured at constant RH = 90% for 3D ep-POP. The temperature is varied between 30 and 70 °C for 40 cycles for consecutive adsorption and desorption isotherms. (c) Gravimetric water sorption experiments of 2D and 3D ep-POPs in the temperature range of 5-45°C. Reprinted with permission from Ref. [75].

REVIEW

the entire cycle and COP-120 showed good reversibility without any performance loss.

Most recently, Byun and Coskun^[75] reported the synthesis of epoxy-functionalized porous organic polymers (ep-POPs) through a catalysis-free, one pot Diels-Alder cycloaddition polymerization (Figure 14a). In the volumetric water uptake experiments, ep-POPs presented hydrophilic characteristics with continuous increase in the entire pressure range. At 90% RH, ep-POPs showed water uptake capacities as high as 41.1 wt%, which was attributed to their high surface area as well as efficient hydrogen-bonding interactions between epoxy moieties and water molecules. Also, the pore size of ep-POPs is slightly larger than the kinetic diameter of a water molecule (2.6 Å), thus allowing easy diffusion of water molecules within the pores in the entire region of the relative humidity. By measuring water sorption isotherms at 298 and 313 K, isosteric heats of adsorption (Q_{st}) values for water adsorption were calculated for 2D (48.1 kJ mol⁻¹) and 3D ep-POP (59.6 kJ mol⁻¹). These Q_{st} values enabled low regeneration temperatures for 2D ep-POP (55 °C) and 3D ep-POP (100 °C). The cycling experiments are illustrated in Figure 14b for 3D ep-POP. 3D ep-POP is exposed to 90% RH using N₂ as a carrier gas. The temperature was varied between 40 and 70 °C for 40 cycles and 3D ep-POP showed exceptional water stability with no loss in water uptake capacity. Additionally, as described in the earlier section for potential applications, each water sorption application has desired temperature and humidity range. Therefore, for practical applications, the desiccants should retain their high uptake capacity under a broad range of temperatures. In this regard, The authors also presented gravimetric water sorption isotherms in various temperatures ranging from 5 to 45 °C at constant 90% RH (Figure 14c). Both 2D and 3D ep-POPs showed almost constant uptake in the entire temperature range with working capacities of 39.2-42.4 wt% and 39.9-41.7 wt% for 2D ep-POP and 3D ep-POP, respectively. The authors emphasized three inherent properties of ep-POPs that can allow exceptional water capture properties; (i) the ideal pore size of ep-POPs allows easy diffusion of water molecules within the pores in the entire relative humidity range; (ii) epoxy functionality is the ideal binding site for water molecules via hydrogen bonding, which provides good reversibility and low regeneration temperatures; (iii) the high content of binding sites allows almost constant uptake in the broad temperature range. Notably, ep-POPs can be applied regardless of geographical region in which they are applied due to their good cycling performance over a wide temperature range along with a low activation temperature.

4. Summary and Outlook

The water vapor adsorption within the cavities of nanoporous materials is manifested by its sensitivity and selectivity towards the surface functionalities, porous structure, structural morphology, hydrophilicity and hydrophobicity. In this review, the current discoveries pertaining to nanoporous adsorbent materials for water vapor adsorption and the mechanisms associated with the sorption profile along with emphasis on the structural modification strategies are presented. The access of water molecules into the nanosized pores within the nanoporous materials incorporating various functional groups opened up a

new class of desiccant materials that combine unique capabilities emergent from the combination of porosity with the hydrophilic functional groups. Accordingly, we highlighted some of the recent progress in understanding the structural properties of nanoporous materials such as zeolites, nanoporous carbons, crystalline and amorphous porous organic polymers (Table 1), that dictate and ultimately lead to their intrinsic desiccant properties. The water sorption ability of nanoporous materials is mainly related to their hydrophilicity, which primarily originates from heteroatoms such as, boron, nitrogen, oxygen, metals and charged atoms present in their backbone. Metal organic frameworks (MOFs) and MOF based hybrid materials certainly showed high water adsorption capacities along with low regeneration temperatures, however, the development of metal-free porous organic polymers having high surface areas and functional elements are highly desirable for water adsorption because of environmental sustainability and to avoid any metal contamination as well as to realize easy regeneration of adsorbents. The hydrophilicity/hydrophobicity, molecular dimensions, connectivity and dynamic interaction of porous organic polymers with water molecules can be regulated by the judicious selection of the building blocks. A variety of porous organic polymers POPs having various heteroatoms have already been reported, and their investigation in the context of water vapor capture would certainly allow us to establish in-depth understanding on the potential of these materials.

The water adsorption ability of porous organic polymers is related to the presence of high microporosity, high pore volume, amount/nature of functional groups and their distinctive interactions with the water molecules. Incorporation of polar organic functionalities or ions within porous organic polymers without compromising their microporous structure and high surface areas is proven to be an efficient strategy to enhance the water adsorption capacity and selectivity. The degree of hydrophilicity in porous organic polymers can be varied by introducing nitrogen and oxygen functionalities including triazine, amine, imine, hydroxy and epoxy functional groups. The water vapor sorption on POPs heavily depends on the interaction of water molecules with the functional groups rather than the surface area and pore volume. The porous organic polymers can be also processed into various shapes/form for their integration into water capture/separation systems such as polymer membranes and adsorbent particles in composite membranes. The advantages of porous organic polymers for water vapour adsorption in comparison to the other adsorbents can be listed as their simple preparation methods, metal free nature, easy incorporation of hydrophilic functional groups, high water stability, low regeneration temperatures, light weight and the high microporosity with tunable textural/structural properties. Although considerable advances have been made for water adsorption using porous organic polymers, the research is still in its infancy and further research efforts needed to develop new catalysts-free polymerization strategies, which can allow simultaneous incorporation of high amount of heteroatoms as well as high surface areas. In addition, any polymerization reaction should be scalable, and low-cost. The design of micron-sized porous organic polymer beads or polymer thin films/membranes which can reversibly adsorb a very large amount of water within a narrow relative humidity window with long term stability, adsorption kinetics, heat transferability, and shaping/processing are important aspects, which still need to be investigated in-depth.

REVIEW

Moreover, considering the competitive binding between CO₂ and H₂O molecules for the flue gas separation, understanding the water uptake behavior of porous organic polymers could enable simultaneous realization of hydrophobicity and CO₂-philicity.

It is clear that the future of porous organic polymers in this emerging area is bright and their unique structural features render them as highly promising candidates for desiccation ranging from atmospheric water capture to various manufacturing process.

Accepted Manuscript

REVIEW

Table 1. Summary of textural properties such as BET surface area, pore volume and pore diameter of selected sorbents along with their water vapor uptake.

Adsorbents	BET Surface Area ^[a] (m ² g ⁻¹)	Micropore volume (cm ³ g ⁻¹)	Total pore volume (cm ³ g ⁻¹)	Average pore diameter (nm)	H ₂ O adsorption ^[b,c] (mmol g ⁻¹)	H ₂ O adsorption ^[b,c] (wt%)	Degassing Temperature (K)	Note	Measured Temperature (K)	Ref.
Covalent Organic Frameworks (COFs)										
AB-COF	1125		0.47	1.3	22.9	41	vacuum		288, 298	[47]
ATFG-COF	520		0.5	0.6, 1.3	13.6	25	vacuum		288, 298	[47]
trzn-COF	408.5		0.21	2.3	2	4	vacuum		298, 308	[48]
TpPa-1	984			1.8	24.5	44	423		298	[49]
TpPa-2	460			1.5	12.5	22	423		298	[49]
TpPa-F ₄	529			1.7	10.1	18	423		298	[49]
TpPa-NO ₂	457			1.6	30	17	423		298	[49]
TpBD	341			2.4	8.1	15	423		298	[49]
TpBD-Me ₂	N/A			N/A	7.5	14	423		298	[49]
TpBD-(OMe) ₂	365			2.3	9.1	16	423		298	[49]
TpBD-(NO ₂) ₂	90			2.2	4.7	9	423		298	[49]
Tp-azo	942			2.7	22.7	41	423		298	[49]
2,5-DhaTab	N/A			N/A	N/A	N/A	423		298	[49]
2,5-DhaTph	1112			2	24.3	44	423		298	[49]
2,3-DhaTph	659			2	8.5	15	423		298	[49]
TpPa-1	1432			1.48	28.9	52	273		298	[50]
TpPa-2	538			1.06	17.3*	31*	273		298	[50]
TpPa-NO ₂	850			1.32	27.2*	49*	273		298	[50]
TpBD	1400			2.18	33.7*	61	273		298	[50]
TpBD-Me ₂	3109			1.63	21*	38*	273		298	[50]
TpBD-(NO ₂) ₂	769			1.63	21*	38*	273		298	[50]
TpBD-(OMe) ₂	1343			1.63	20.8*	37*	273		298	[50]
Tp-Azo	3038			2.58	27.1	49	273		298	[50]
TpAnq	1027			1.63	21.8*	39*	273		298	[50]
TpBpy	2336			2.42	43.5	78	273		298	[50]
TpTph	1020			2.58	19.3*	35*	273		298	[50]
TpTta	825			0.86	19.3*	35*	273		298	[50]

REVIEW

Covalent Triazine Frameworks (CTFs)

CE-1	960	0.126	0.97	0.82	12.3*	22*	423		293	[57]
CE-2	588	0.155	0.47	0.78	3.9*	6.9*	423		293	[57]
CE-3	540	0.14	0.43	0.86	3.5*	6.3*	423		293	[57]
bipy-CTF500	1548	0.64	0.71	0.8	25.1*	45*	vacuum		298	[58]
pym-CTF500	208	N/A	N/A	0.8	12.2*	22*	vacuum		298	[58]
CTF-a	2439		1.96		77.2	139	vacuum		292.5	[59]
CTF-b	1179		0.64		31.3	56	vacuum		292.5	[59]
CTF-c	2071		1.36		50.9	91.8	vacuum		292.5	[59]
CTF-d	1683		2.63		41.7	75	vacuum		292.5	[59]
CTF-TPC	1668	0.65	0.93	0.59	19.0*	34*	403		293	[60]
CTF-FL	773	0.31	0.39	0.5	11.7*	21*	403		293	[60]
Ad2L1	918	0.34	0.86		15.5	28	473		293	[61a]
Ad2L2	1316	0.48	2.2		8.9	16	473		293	[61a]
Ad2L3	747	0.28	0.45		12.8	23	473		293	[61a]
Ad3L1	1199	0.44	0.8		23.9	43	473		293	[61a]
Ad3L2	1093	0.4	0.96		21.1	38	473		293	[61a]
Ad3L3	1328	0.48	0.93		31.1	56	473		293	[61a]
Ad4L1	1617	0.61	0.9		25.0	45	473		293	[61a]
Ad4L2	1885	0.67	1.52		38.3	69	473		293	[61a]
Ad4L3	1341	0.52	0.74		30.0	54	473		293	[61a]
MM1	1800	0.67	1.11		27.7	50	473 5.1 wt% by KTF Method		293	[61b]
MM2	1360	0.55	0.67		24.5	44	473 17.5 wt% by KTF Method		293	[61b]
MM3	1884	0.67	1.52		42.3	76	473 1.9 wt% by KTF Method		293	[61b]
MM4	1407	0.54	0.78		21.4	38	473 6.3 wt% by KTF Method		293	[61b]
bpim-CTF-300	2.4	-			6.4	11.5	423		298	[63]
bpim-CTF-400	786	0.33	0.34		17.1	30.7	423		298	[63]
bpim-CTF-500	1556	0.74	0.75		26.8	48.2	423		298	[63]
DCBP-CTF-1	2437	1.41	1.48		28.13	50.7	423		293	[64]
F-DCBP-CTF-1	1574	0.51	1.5		11.3	20.3	423		293	[64]

REVIEW

Porous Organic Polymers (POPs)										
CPOP-8	1610 (430)		1.71	0.63	6.7*	12*	393		298	[65]
CPOP-9	2440 (180)		2.04	0.63	24.6*	44*	393		298	[65]
CPOP-10	1110 (650)		0.76	0.63	2.2*	4*	393		298	[65]
CPOP-11	1320		1.13	0.61, 1.33	1.1*	2*	393		298	[66]
CPOP-12	1180		1.05	0.59, 1.31	8.4*	15*	393		298	[66]
PSN-3	865	0.83		0.6	3.3*	6*	393		298	[67]
MPI-6FA	781		0.53	0.48	4.7 at 80RH	8.5 at 80RH	393		298	[68]
MPI-BPA	677		0.39	0.53	7.4 at 80RH	13.3 at 80RH	393		298	[68]
MPI-BTA	490		0.53	0.53	5.8 at 80RH	10.4 at 80RH	-		298	[68]
KFUPM-1	305			1	18.7	33.5	383		298	[69]
NU-POP-1	950		0.32	0.35-0.8	12.8*	23*	-		298	[70]
OFC-1	780		0.54		6.8*	12.2*	423		298	[71]
DUT-92	720		1.76		4.5*	8.1*	423		298	[71]
DUT-92 (NO ₂)	500		0.44		8.1*	14.5*	423		298	[71]
DUT-92 (NH ₂)	700		0.42		13.7*	24.5*	423		298	[71]
DUT-93	320		1.02		2.2*	3.9*	423		298	[71]
DUT-93 (NO ₂)	160		0.5		5.4*	9.6*	423		298	[71]
DUT-93 (NH ₂)	nonporous		nonporous		9.0*	16.1*	423		298	[71]
MOPI-I	206	0.05	0.16		13.5	24.192	383		298	[73]
MOPI-II	644	0.17	0.32		12.3	22.0	383		298	[73]
MOPI-III	433	0.09	0.27		9.0	16.1	383		298	[73]
MOPI-IV	660	0.19	0.28		19.5	34.4	383		298	[73]
MOPI-V	921	0.23	0.44		7.0	12.5	383		298	[73]
PIN1	458	0.5	0.3	0.6	8.5	15.2	423		298	[72]
PIN2	325	0.17	0.35		7.0	12.5	423		298	[72]
PIN1_2	28	-	0.05		3.0	5.4	423		298	[72]
COP-120	42		0.15		25.1*	45*	383		298	[74]
2D ep-POP	852 (464)	0.18		0.47	22.9	41.1	Regeneration at 328 K		298	[75]
3D ep-POP	779 (462)	0.17		0.4	22.9	41.1	Regeneration at 100 °C		298	[75]
EOF-6 (POP)	1380	0.9	0.63		19.5	35	423		298	[76]
EOF-7 (POP)	1083	0.69	0.51		4.9	8.8	423		298	[76]
EOF-8 (POP)	540	0.32	0.26		2.0	3.6	423		298	[76]
EOF-9 (POP)	602	0.38	0.3		4.9	8.8	423		298	[76]
Py-PP			0.71		1.1	2	483		298	[77]

[a] Values in bracket is Micropore surface area

[b] Vapour uptake at $P/P_0=0.9$

[c] Approximate values from the isotherm graphs are marked with *

REVIEW

Acknowledgements

The authors acknowledge the support by the Basic Science Research Program through the National Research Foundation of Korea (NRF) funded by the Ministry of Education (2017R1A6A3A01005029).

Keywords: porous organic polymers • water vapor capture • organic desiccants • CO₂ separation • Surface area

- [1] M. S. Shafeeyan, W. M. A. W. Daud, A. Houshamd, A. Shamiri, *J. Anal. Appl. Pyrolysis* **2010**, *89*, 143-151.
- [2] B. M. Weckhuysen, J. Yu, *Chem. Soc. Rev.* **2015**, *44*, 7022-7024.
- [3] a) S. S. Chui, S. M.-F. Lo, J. P. H. Charmant, A. G. Orpen, I. D. Williams, *Science* **1999**, *283*, 1148-1150; b) H. Li, M. Eddaoudi, M. O'Keeffe, O. M. Yaghi, *Nature* **1999**, *402*, 276-279.
- [4] A. P. Cote, A. I. Benin, N. W. Ockwig, M. O'Keeffe, A. J. Matzger, O. M. Yaghi, *Science* **2005**, *310*, 1166-1170.
- [5] S. Das, P. Heasman, T. Ben, S. Qiu, *Chem. Rev.* **2017**, *117*, 1515-1563.
- [6] R. Shenhar, T. B. Norsten, V. M. Rotello, *Adv. Mater.* **2005**, *17*, 657-669.
- [7] P. Li, J. A. Modica, A. J. Howarth, E. L. Vargas, P. Z. Moghadam, R. Q. Snurr, M. Mrksich, J. T. Hupp, O. K. Farha, *Chem* **2016**, *1*, 154-169.
- [8] M. O. Adebajo, R. L. Frost, J. T. Kloprogge, O. Carmody, S. Kokot, *J. Porous Mater.* **2003**, *10*, 159-170.
- [9] K. S. W. Sing, D. H. Everett, R. A. W. Haul, L. Moscou, R. A. Pierotti, J. Rouquerol, T. Siemieniewska, *Pure Appl. Chem.* **1985**, *57*, 603-619.
- [10] A. M. Ribeiro, T. P. Sauer, C. A. Grande, R. F. P. M. Moreira, J. M. Loureiro, A. E. Rodrigues, *Ind. Eng. Chem. Res.* **2008**, *47*, 7019-7026.
- [11] D. Ferreira, R. Magalhaes, P. Taveira, A. Mendes, *Ind. Eng. Chem. Res.* **2011**, *50*, 10201-10210.
- [12] P. Kanchanalai, R. P. Lively, M. J. Realff, Y. Kawajiri, *Ind. Eng. Chem. Res.* **2013**, *52*, 11132-11141.
- [13] a) A. A. Askalany, M. Salem, I. M. Ismael, A. H. H. Ali, M. G. Morsy, B. B. Saha, *Renewable Sustainable Energy Rev.* **2013**, *19*, 565-572; b) H. Demir, M. Mobedi, S. Ulku, *Renewable Sustainable Energy Rev.* **2008**, *12*, 2381-2403; c) M. S. Fernandes, G. J. V. N. Brites, J. J. Costa, A. R. Gaspar, V. A. F. Costa, *Renewable Sustainable Energy Rev.* **2014**, *39*, 102-123; d) M. Sultan, I. I. El-Sharkawy, T. Miyazaki, B. B. Saha, S. Koyama, *Renewable Sustainable Energy Rev.* **2015**, *46*, 16-29.
- [14] E. P. Ng, S. Mintova, *Microporous Mesoporous Mater.* **2008**, *114*, 1-26.
- [15] N. C. Srivastava, I. W. Eames, *Appl. Therm. Eng.* **1998**, *18*, 707-714.
- [16] N. C. Burtch, H. Jasuja, K. S. Walton, *Chem. Rev.* **2014**, *114*, 10575-10612.
- [17] S. Lowell, J. E. Shields, M. A. Thomas, M. Thommes, *Characterization of Porous Solids and Powders: Surface Area, Pore Size and Density*, Vol. 16, Springer Netherlands, **2004**.
- [18] M. W. Anderson, J. Klinowski, *J. Chem. Soc., Faraday Trans. 1* **1986**, *82*, 1449-1469.
- [19] P. K. J. Weitkamp, A. Kiss, C.H. Berke, in: R. von, J. B. H. Ballmoos, M.M.J. Treacy (Eds.), *Proc. Ninth Int. Zeol. Conf.*, Butterworth-Heinemann, Stoneham, MA, **1993**.
- [20] A. Giaya, R. W. Thompson, R. Denkewicz, *Microporous Mesoporous Mater.* **2000**, *40*, 205-218.
- [21] J. Canivet, A. Fateeva, Y. Guo, B. Coasne, D. Farrusseng, *Chem. Soc. Rev.* **2014**, *43*, 5594-5617.
- [22] a) P. D. Sullivan, B. R. Stone, Z. Hashisho, M. J. Rood, *Adsorption-Journal of the International Adsorption Society* **2007**, *13*, 173-189; b) K. V. Kumar, K. Preuss, Z. X. Guo, M. M. Titirici, *J. Phys. Chem. C* **2016**, *120*, 18167-18179.
- [23] Ashrae, *2015 ASHRAE Handbook-HVAC Applications*, Ashrae, Atlanta, **2015**.
- [24] T. C. Drage, C. E. Snape, L. A. Stevens, J. Wood, J. Wang, A. I. Cooper, R. Dawson, X. Guo, C. Satterley, R. Irons, *J. Mater. Chem.* **2012**, *22*, 2815-2823.
- [25] S. Mintova, S. Y. Mo, T. Bein, *Chem. Mater.* **2001**, *13*, 901-905.
- [26] D. H. Olson, W. O. Haag, W. S. Borghard, *Microporous Mesoporous Mater.* **2000**, *35-6*, 435-446.
- [27] a) B. Hunger, O. Klepel, C. Kirschhock, M. Heuchel, H. Toufar, H. Fuess, *Langmuir* **1999**, *15*, 5937-5941; b) F. M. Higgins, N. H. de Leeuw, S. C. Parker, *J. Mater. Chem.* **2002**, *12*, 124-131.
- [28] M. Tatlier, G. Munz, S. K. Henninger, *Microporous Mesoporous Mater.* **2018**, *264*, 70-75.
- [29] a) L. F. Scatena, M. G. Brown, G. L. Richmond, *Science* **2001**, *292*, 908-912; b) K. Koga, G. T. Gao, H. Tanaka, X. C. Zeng, *Nature* **2001**, *412*, 802-805.
- [30] L. Liu, S. J. Tan, T. Horikawa, D. D. Do, D. Nicholson, J. Liu, *Adv. Colloid Interface Sci.* **2017**, *250*, 64-78.
- [31] Y. Tao, H. Muramatsu, M. Endo, K. Kaneko, *J. Am. Chem. Soc.* **2010**, *132*, 1214-1215.
- [32] T. Ohba, *Angew. Chem. Int. Ed.* **2014**, *53*, 8032-8036.

REVIEW

- [33] O. T. K. H, Y. M, I. S, K. K, in *In: CD proceedings of the international carbon conference, Biarritz, France, 2009.*
- [34] H. Sakamoto, T. Fujimori, X. L. Li, K. Kaneko, K. Kan, N. Ozaki, Y. Hijikata, S. Irle, K. Itami, *Chem. Sci.* **2016**, 7, 4204-4210.
- [35] M. Nakamura, T. Ohba, P. Branton, H. Kanoh, K. Kaneko, *Carbon* **2010**, 48, 305-308.
- [36] T. Horikawa, T. Muguruma, D. D. Do, K. I. Sotowa, J. R. Alcantara-Avila, *Carbon* **2015**, 95, 137-143.
- [37] M. Thommes, J. Morell, K. A. Cychosz, M. Froba, *Langmuir* **2013**, 29, 14893-14902.
- [38] P. Lodewyckx, *Carbon* **2010**, 48, 2549-2553.
- [39] N. Qi, M. D. LeVan, *Carbon* **2005**, 43, 2258-2263.
- [40] D. D. Do, S. Junpirom, H. D. Do, *Carbon* **2009**, 47, 1466-1473.
- [41] L. Cossarutto, T. Zimny, J. Kaczmarczyk, T. Siemieniewska, J. Bimer, J. V. Weber, *Carbon* **2001**, 39, 2339-2346.
- [42] T. Ohba, K. Kaneko, *Langmuir* **2011**, 27, 7609-7613.
- [43] G. P. Hao, G. Mondin, Z. Zheng, T. Biemelt, S. Klosz, R. Schubel, A. Eychmuller, S. Kaskel, *Angew. Chem. Int. Ed.* **2015**, 54, 1941-1945.
- [44] X. L. Sun, G. P. Hao, X. Y. Lu, L. X. Xi, B. Liu, W. P. Si, C. S. Ma, Q. M. Liu, Q. Zhang, S. Kaskel, O. G. Schmidt, *J. Mater. Chem. A* **2016**, 4, 10166-10173.
- [45] E. Zhang, G. P. Hao, M. E. Casco, V. Bon, S. Gratz, L. Borchardt, *J. Mater. Chem. A* **2018**, 6, 859-865.
- [46] G. P. Hao, N. R. Sahraie, Q. Zhang, S. Krause, M. Oschatz, A. Bachmatiuk, P. Strasser, S. Kaskel, *Chem. Commun.* **2015**, 51, 17285-17288.
- [47] L. Stegbauer, M. W. Hahn, A. Jentys, G. Savasci, C. Ochsenfeld, J. A. Lercher, B. V. Lotsch, *Chem. Mater.* **2015**, 27, 7874-7881.
- [48] D. Mullangi, S. Nandi, S. Shalini, S. Sreedhala, C. P. Vinod, R. Vaidhyanathan, *Sci. Rep.* **2015**, 5, 10876.
- [49] B. P. Biswal, S. Kandambeth, S. Chandra, D. B. Shinde, S. Bera, S. Karak, B. Garai, U. K. Kharul, R. Banerjee, *J. Mater. Chem. A* **2015**, 3, 23664-23669.
- [50] S. Karak, S. Kandambeth, B. P. Biswal, H. S. Sasmal, S. Kumar, P. Pachfule, R. Banerjee, *J. Am. Chem. Soc.* **2017**, 139, 1856-1862.
- [51] P. Kuhn, M. Antonietti, A. Thomas, *Angew. Chem. Int. Ed.* **2008**, 47, 3450-3453.
- [52] S. Ren, M. J. Bojdys, R. Dawson, A. Laybourn, Y. Z. Khimyak, D. J. Adams, A. I. Cooper, *Adv. Mater.* **2012**, 24, 2357-2361.
- [53] S. N. Talapaneni, T. H. Hwang, S. H. Je, O. Buyukcakir, J. W. Choi, A. Coskun, *Angew. Chem. Int. Ed.* **2016**, 55, 3106-3111.
- [54] S. Y. Yu, J. Mahmood, H. J. Noh, J. M. Seo, S. M. Jung, S. H. Shin, Y. K. Im, I. Y. Jeon, J. B. Baek, *Angew. Chem. Int. Ed.* **2018**.
- [55] K. Wang, L. M. Yang, X. Wang, L. Guo, G. Cheng, C. Zhang, S. Jin, B. Tan, A. Cooper, *Angew. Chem. Int. Ed.* **2017**, 56, 14149-14153.
- a) M. Liu, Q. Huang, S. Wang, Z. Li, B. Li, S. Jin, B. Tan, *Angew. Chem. Int. Ed.* **2018**, 57, 11968-11972; b) M. Liu, K. Jiang, X. Ding, S. Wang, C. Zhang, J. Liu, Z. Zhan, G. Cheng, B. Li, H. Chen, S. Jin, B. Tan, *Adv. Mater.* **2019**, doi.org/10.1002/adma.201807865
- H. Yu, C. J. Shen, M. Z. Tian, J. Qu, Z. G. Wang, *Macromolecules* **2012**, 45, 5140-5150.
- S. Hug, L. Stegbauer, H. Oh, M. Hirscher, B. V. Lotsch, *Chem. Mater.* **2015**, 27, 8001-8010.
- J. Artz, R. Palkovits, *ChemSusChem* **2015**, 8, 3832-3838.
- S. Dey, A. Bhunia, D. Esquivel, C. Janiak, *J. Mater. Chem. A* **2016**, 4, 6259-6263.
- a) S. Dey, A. Bhunia, I. Boldog, C. Janiak, *Microporous Mesoporous Mater.* **2017**, 241, 303-315; b) S. Dey, A. Bhunia, H. Breitzke, P. B. Groszewicz, G. Buntkowsky, C. Janiak, *J. Mater. Chem. A* **2017**, 5, 3609-3620.
- O. Buyukcakir, S. H. Je, S. N. Talapaneni, D. Kim, A. Coskun, *ACS Appl. Mater. Interfaces* **2017**, 9, 7209-7216.
- K. Park, K. Lee, H. Kim, V. Ganesan, K. Cho, S. K. Jeong, S. Yoon, *J. Mater. Chem. A* **2017**, 5, 8576-8582.
- G. B. Wang, K. Leus, H. S. Jena, C. Krishnaraj, S. N. Zhao, H. Depauw, N. Tahir, Y. Y. Liu, P. Van der Voort, *J. Mater. Chem. A* **2018**, 6, 6370-6375.
- Q. Chen, D. P. Liu, J. H. Zhu, B. H. Han, *Macromolecules* **2014**, 47, 5926-5931.
- L. J. Feng, Q. Chen, J. H. Zhu, D. P. Liu, Y. C. Zhao, B. H. Han, *Polym. Chem.* **2014**, 5, 3081-3088.
- G. Li, B. Zhang, Z. Wang, *Macromol. Rapid Commun.* **2014**, 35, 971-975.
- G. Y. Li, B. Zhang, J. Yan, Z. G. Wang, *J. Mater. Chem. A* **2016**, 4, 11453-11461.
- M. M. Abdelnaby, A. M. Alloush, N. A. A. Qasem, B. A. Al-Maythalony, R. B. Mansour, K. E. Cordova, O. C. S. Al Hamouz, *J. Mater. Chem. A* **2018**, 6, 6455-6462.
- G. W. Peterson, O. K. Farha, B. Schindler, P. Jones, J. Mahle, J. T. Hupp, *J. Porous Mater.* **2012**, 19, 261-266.
- F. M. Wisser, K. Eckhardt, D. Wisser, W. Bohlmann, J. Grothe, E. Brunner, S. Kaskel, *Macromolecules* **2014**, 47, 4210-4216.
- N. Popp, T. Homburg, N. Stock, J. Senker, *J. Mater. Chem. A* **2015**, 3, 18492-18504.
- C. Klumpen, M. Breunig, T. Homburg, N. Stock, J. Senker, *Chem. Mater.* **2016**, 28, 5461-5470.

REVIEW

- [74] J. Byun, H. A. Patel, D. Thirion, C. T. Yavuz, *Polymer* **2017**, *126*, 308-313.
- [75] Y. Byun, A. Coskun, *Angew. Chem. Int. Ed.* **2018**, *57*, 3173-3177.
- [76] M. Rose, N. Klein, W. Böhlmann, B. Böhringer, S. Fichtner, S. Kaskel, *Soft Matter* **2010**, *6*, 3918-3923.
- [77] K. V. Rao, S. Mohapatra, T. K. Maji, S. J. George, *Chem. Eur. J.* **2012**, *18*, 4505-4509.

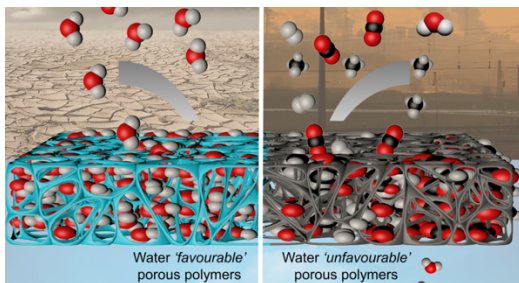
Accepted Manuscript

REVIEW

Entry for the Table of Contents (Please choose one layout)

Layout 2:

REVIEW



Yearin Byun, Sang Hyun Je, Siddulu Naidu Talapaneni, and Ali Coskun*

Page No. – Page No.

Advances in Porous Organic Polymers for Efficient Water Capture